# Electromechanical Phenomena in Ice

Victor F. Petrenko

*Abstract*

This report examines the electromechanical effects in ice. This group of physical phenomena, which was found and studied relatively recently, broadens basic knowledge of ice and may have some practical applications. The electromechanical phenomena in this monograph are separated into three groups: 1) Effects in which electromagnetic fields are generated by means of mechanical actions such as elastic stress, plastic strain, fracture or friction; 2) Effects in which an application of electric fields modifies such mechanical properties of ice as its plasticity, elasticity and friction; 3) Effects in which plastic strain changes electrical conductivity or dielectric permittivity of ice. Experimental results and theoretical models are discussed and some possible practical applications suggested.

**US Army Corps
of Engineers**
Cold Regions Research &
Engineering Laboratory

# Electromechanical Phenomena in Ice

Victor F. Petrenko                                    February 1996

## PREFACE

# CONTENTS

# ILLUSTRATIONS

Figure

# FOREWORD

At the present time, thousands and thousands of people around the world deal with ice, snow and permafrost. They are scientists, educators, engineers, navigators, meteorologists and others. While a small fraction of these people contribute to the knowledge base in ice physics, all of them use knowledge from it frequently. Moreover, successful applied research is based upon fundamental science—one more reason for ice specialists to have a textbook on ice physics on their desks.

The first modern ice physics text was Fletcher's book on *The Chemical Physics of Ice* (1970). Fletcher's book is in typical textbook format: it is reasonably brief and easy to understand. He touched on a few of the most important topics, but not all of them.

The most comprehensive book on ice physics to date was published by Hobbs in 1974. Hobbs considered almost all of the basic aspects of ice as understood at that time. Moreover, he described and compared several (sometimes opposing) viewpoints. This fundamental and rather large (837 pages) book is commonly known as the "Ice Bible" by specialists in the field. In 1974 and 1975, two CRREL Monographs on ice were produced by John Glen. These were briefly and clearly written and reviewed almost all ice-related subjects. This work was (and in some respects still is) a magnificent introduction to ice.

Finally, in 1981 Maeno wrote a simple, popular book for the express purpose of attracting people's attention to the subject.

During the past 20 years, a significant amount of new experimental and theoretical work has appeared, dramatically changing our views on ice physics. As a result, we are now able to formulate physical laws using more simple and direct methods. We have found some of the physical models used in the past to be completely wrong. The physics of ice is a much better developed subject than it was 20 years ago.

For the above reasons, I feel the time is ripe for a contemporary book on ice physics, incorporating the known and proven with almost 20 years worth of material not covered by previous works.

I have tried to prepare a "readable" book, and not one that requires the reader to be a uniquely educated person. It is my intent to present the material in such a way that any reader attracted by the title *Ice Physics* will be able to comprehend it. This is quite difficult for a book dedicated, not to a particular field of knowledge, but to a specific material. Indeed, for ice it means we have to consider a wide variety of subjects, including quantum chemistry, solid state physics, the theory of elasticity, ionic conductivity, synchrotron x-ray topography, crystal growth, the physics of surfaces and more.

The primary goal is to produce as simple a book as possible without sacrificing scientific accuracy. Experimental facts, physical ideas and theories will be strongly organized and bound together cohesively. The reader will be introduced to a wide variety of material on a step by step basis. Then the picture will be whole.

To accelerate materials publication, this book will appear first in the form of a series of joint CRREL–Dartmouth reports, later to be published in CRREL's Monograph series, on:

1. The structure of ordinary ice
   Part I: "Ideal" structure of ice. Ice crystal lattice
   Part II: Defects in Ice
      Volume 1: Point defects
      Volume 2: Dislocations and planar defects
2. Electrical properties of ice
   Part I: Conductivity and dielectric permittivity of ice
   Part II: Advanced topics and new physical phenomena
3. Optical properties
4. Electro–optical effects in ice
5. Thermal properties
6. Mechanical properties of ice. Elasticity and anelastic relaxation. Plastic properties. Fracture of ice
7. Electromechanical phenomena in ice
8. Surface of ice
9. Other forms of ice and their properties
10. Ice in space
11. Ice research laboratories

The reports will be prepared in a sequence convenient to the author. The present report is the sixth in the series.

## NOMENCLATURE

| | |
|---|---|
| α | angle |
| $a$ | interatomic distance |
| $\alpha_{ai}$ | deformation-potential constant of $i^{th}$ type charge carrier |
| $\alpha_0$ | fraction of water molecules on the ice surface oriented with their dipole moments (i.e., protons) pointing outwards |
| $C, C_0$ | capacitance |
| $\chi_{ij}$ | susceptibility tensor |
| $c_{mnij}$ | stiffness tensor |
| $\Delta$ | thickness of the surface layer |
| $\Delta I$ | dislocation current |
| $d$ | interelectrode distance |
| $D_i$ | diffusion coefficient of $i^{th}$ defects |
| $D_{ion}$ | diffusion coefficient of ions |
| $d_{kmn}$ | piezoelectric strain tensor |
| $E$ | electric field strength |
| $E_\perp$ | component of electric field perpendicular to a crack surface |
| **E** | Young's modulus |
| ε | dielectric permittivity |
| $e$ | proton charge |
| $\varepsilon_0$ | dielectric permittivity of a vacuum |
| $E_{ai}$ | activation energy of a defect |
| $E_i$ | $i^{th}$ component of the electric field strength |
| $e_i$ | defects' electric charge ($i = 1, 2, 3, 4$) |
| $e_{ion}$ | electric charge of an ion |
| $\varepsilon_{ij}$ | strain tensor |
| $e_{ijk}$ | piezoelectric stress tensor |
| $\varepsilon_s$ | static dielectric permittivity of ice |
| $\varepsilon_\infty$ | high-frequency dielectric permittivity of ice |
| $F$ | force |
| $\Phi$ | $\cong 3.85 k_B\, T\, r_{oo}$ |
| $f$ | frequency |
| $g$ | grain size |
| $\gamma_{ai}$ | activation volume of a defect creation |
| $H$ | magnetic field |

| | |
|---|---|
| η | amplitude of dislocation vibrations |
| $I$ | electric current |
| $i$ | 1, 2 ,3 |
| $j_D$ | diffusion flux |
| $J_{DR}$ | drift flux |
| $j_i$ | flux of $i^{th}$ defects |
| $\varphi_s$ | surface potential |
| $\kappa_1^{-1}, \kappa_2^{-1}$ | screening lengths |
| $k_B$ | Boltzmann constant |
| $K_I$ | intensity factor for a mode I crack |
| $K_{II}$ | intensity factor for a mode II crack |
| $L$ | film thickness |
| $l$ | length of a crack |
| $\lambda, \lambda_s, \lambda_{ski}$ | surface charge density |
| $l_d$ | length of a dislocation segment |
| $\lambda_{sc}$ | screening charge density |
| $L_t$ | length of electrically charged track |
| μ | friction coefficient |
| $\mu_i$ | mobility of $i^{th}$ defect |
| $\mu_{ion}$ | mobility of ions |
| $n$ | concentration |
| **ν** | Poisson's ratio |
| $n_1$ | $H_3O^+$ ion concentration |
| $n_2$ | $OH^-$ ion concentration |
| $n_3$ | D-defect concentration |
| $n_4$ | L-defect concentration |
| $N$ | water molecules' concentration |
| $P$ | pressure |
| $P_0$ | normal pressure |
| $P_o$ | polarization |
| $P_{el}$ | electrostatic pressure |
| $P_i$ | $i^{th}$ component of the polarization vector |
| $Q$ | electric charge |
| θ | angle between a crack plane and $\vec{r}$ |
| $q$ | linear density of dislocation charge |
| $R$ | resistance |
| $r$ | distance to a crack tip |
| ρ | space charge density |

| | | | | |
|---|---|---|---|---|
| $\rho_i$ | dipole moment of water molecule | $\tau_2$ | slow electric relaxation time |
| $s$ | surface area | $\tau_D$ | Debye relaxation time |
| $\sigma(\infty)$ | tensile stress at infinity | $u$ | potential energy of a defect |
| $\sigma_{ij}$ | stress tensor | $V$ | potential difference or applied voltage |
| $s_{mnij}$ | compliance tensor | $v_{cr}$ | crack velocity |
| $\sigma_s$ | ice static conductivity | $\boldsymbol{v}$ | velocity |
| $\sigma_\infty$ | high-frequency conductivity of ice | $\omega_D$ | Debye frequency |
| $T$ | temperature | $x$ | distance to ice surface |
| $T_d$ | tension of a dislocation line | $\vec{E}$ | electric field strength |
| $t$ | time | $\vec{P}$ | polarization vector |
| $\tau(\infty)$ | shear stress at infinity | $\vec{r}$ | pointing vector drawn from a crack tip to the point of observation |
| $\tau_1$ | fast electric relaxation time | | |
| $T_1, T_2$ | belt tension | $\vec{\Omega}$ | configuration vector |

# Electromechanical Phenomena in Ice

VICTOR F. PETRENKO

## INTRODUCTION

Among the numerous interesting properties of ice, there is a group of physical phenomena in which electrical and mechanical properties correlate. That correlation can manifest itself in three ways:

1. Electromagnetic fields are generated by means of mechanical actions, such as elastic stress, plastic strain, fracture or friction.

2. Mechanical properties, such as plasticity, elasticity and friction, are modified by the application of electrical fields.

3. Electrical conductivity or dielectric permittivity are changed by strain.

We will refer to such effects as electromechanical phenomena (EMP). Most of the experimental results described in this report were discovered recently, during the last decade. Of course, ice is not unique in exhibiting electromechanical effects. Similar phenomena were previously found in semiconductors, ferroelectric and piezoelectric materials, where EMP may have a much greater intensity—electrical fields are much stronger, for instance. Nevertheless, EMP in natural ice may have quite a large total magnitude, such as electrical potential difference, owing to the large size typical of ice sheets. In addition, since ice is one of the most widespread materials on Earth, the electromechanical effects described below may have important practical applications.

## ELECTRICAL PHENOMENA IN ICE FRICTION

This section describes two recently discovered effects in friction on ice and snow. The first one is a strong frictional electrification (Petrenko and Colbeck 1995), and the second is an effect of electrical fields on ice friction (Petrenko 1994a). These phenomena illustrate the important role that ice electrical properties plays in ice friction. It is most likely that these effects result from the special structure and electrical properties of the ice surface. Since the physical properties of the ice surface were discussed in detail in a previous report (Petrenko 1994b), we will only briefly review the information necessary to the following discussion.

### Structure and electrical properties of the ice surface

The physical properties of the ice surface differ significantly from those of bulk ice. In the temperature range from 0°C to approximately –4°C, there is a thin liquid or liquid-like film on the ice surface, which has optical properties very similar to those of ordinary water (Furukawa et al. 1987, Elbaum et al. 1993). The film's thickness depends on temperature, surface crystallographic orientation and ice purity. The film is also sensitive to environmental conditions and it is about 50 nm at –1°C. A special layer remains on the ice surface even at temperatures down to –100°C. This layer exhibits a diffusion coefficient, electrical conductivity, structure and viscosity that are quite distinct from those of bulk ice (see Maeno 1973, Barer et al. 1977, Golecki and Jaccard 1978, Mizuno and Hanafuza 1987).

One of the best-known theoretical models developed to explain ice surface structure and properties was invented by Fletcher (1962, 1963, 1968). The key idea in Fletcher's model is the assumption that at the ice surface a significant fraction of molecules (denoted as $\alpha_0$) is oriented with their dipole moments (i.e., protons) pointing outwards, as opposed to the bulk where molecules are oriented randomly. This would result in the buildup of a large positive polarization charge at the surface. Fletcher came to his conclusion about

molecule orientational ordering by analyzing the interaction between dipole and quadruple moments of water molecules close to the surface. Such an orientation of water molecules implies a high density surface electrical charge $\lambda_s$. Though this charge was predicted by Fletcher many years ago, its existence was proven experimentally only recently during experiments on the frictional electrification of ice and snow.

All other predictions of Fletcher's model are consequences of the molecular ordering in the surface layer. In fact, since in the bulk there is no ordering between the surface and the bulk, there should be a transitional layer with a large concentration of hydrogen bond defects allowing molecules to reorient. This transitional disordered layer, according to Fletcher, is the liquid-like layer. Besides the Fletcher model, there have been several others designed to explain the unique physical properties of the ice surface. No one of them is able to account for all of its known properties.

One important surface property is ice friction. The bibliography on ice and snow friction is vast (see reviews by Hobbs [1974] and Colbeck [1992]). Here, we can examine only the major ideas available in the literature on this subject. In doing so, we will underscore the facts that make ice different from most other materials. In static friction, the strong and universal adhesion of ice to almost any solid is one such difference. Depending on temperature, ice/slider interface roughness and slider materials, it takes from a fraction of a second to hours to produce mechanically a very strong ice/solid interface. Intensive mass transport via the liquid-like surface film accelerates this process at temperatures above –10°C. The nature of the strong bonding between ice and solids is not quite understood yet and perhaps originates from the special arrangement of water molecules on the ice surface mentioned above.

The coefficient of kinetic friction of ice in the temperature interval from –3 to –40°C strongly depends on sliding velocity $v$, varying from 0.9 at $v = 10^{-5}$ m/s to 0.05 at $v > 10^{-1}$ m/s (Barnes et al. 1971, Evans et al. 1976, Jones et al. 1991). For granite-on-ice friction, Barnes et al. (1971) distinguish three ranges of sliding velocity characterized by the different mechanisms that govern the friction: ice creep, when $v < 10^{-6}$ m/s; ice plastic flow and fracture, when $10^{-3}$ m/s $> v > 10^{-6}$ m/s; and frictional melting, when $v > 10^{-3}$ m/s, $T = -11.75$°C. The velocity at which the transition to frictional melting takes place may depend on the initial ice temperature, normal pressure and ice and slider roughness, but the occurrence of melting and liquid lubrication of the ice friction have been proven many times. Yet, for a precise quantitative description of such friction, we need more data on both the film thickness and the real contact area. At temperatures close to the melting point and at high normal pressure, the pressure melting of ice can also contribute to the formation of a liquid film between the ice and a slider.

The study of the surface potential of ice and electrical charges at the ice surface has quite a long history and continues to attract the attention of numerous scholars. Such interest in the electrostatic properties of the surface of ice is stimulated by both the fundamental problems associated with it and certain practical issues. Fundamental questions, which the study of the surface potential and ice surface might help to resolve, include the issue of the structure of the surface of ice. For instance, if all the molecules at the ice surface are oriented "proton-outwards" as Fletcher's model suggests, this must lead to a positive charge at the surface $\lambda_s$ and a positive potential of the ice surface $\varphi_s$. Both $\lambda_s$ and $\varphi_s$ are determined by the thickness of the surface layer $\Delta$ and the fraction of the oriented water molecules contained in this layer. Thus, measurement of $\lambda_s$ and $\varphi_s$ in conjunction with other data ($\Delta$ for example) might provide valuable information on the microscopic structure and nature of the ice surface layer.

The practical issues stimulating the study of the electrical properties of the ice surface, include, first of all, the problem of atmospheric electricity (see review in Hobbs 1974) as well as the problem of adhesion and friction of ice and snow (Petrenko 1994a,b).

Among physical mechanisms suggested to explain ice surface charge and thunderstorm electricity were surface electronic states (Buser and Jaccard 1978), a thermoelectrical effect (Latham and Mason 1961, Latham 1963), charge separation on freezing (Workman and Reynolds 1949, 1950), and the motion of charged dislocations produced by rubbing one piece of ice against another (Takahashi 1969a).

**Early works on asymmetrical rubbing**

Until recently, asymmetrical rubbing of ice on ice was the only phenomenon studied in connection with ice frictional electrification. Chalmers (1952) measured an electrical charge from small snow fragments when two handfuls of snow were rubbed together, finding a negative electrical charge of $2–8 \times 10^{-10}$ C on the ice fragments. Yoshida (1944), Reynolds et al. (1957), Latham and Mason (1961) and Latham (1963) studied charge separation during asymmetrical rubbing of ice on ice. In such an experiment, the constant rubbing point becomes warmer than the variable rubbing point. The electrical potential differences generated in such experiments were very small and did not exceed tens of millivolts. Such weak electrification is attributable to the rubbing piece being heated more than the rubbed one, with the potential difference arising from the thermoelectrical effect. Since the thermo-

electrical power of ice does not exceed 4 mV/°C (Bryant and Fletcher 1965), this effect is always small.

Takahashi (1969a) measured the electrical potential difference between a vibrating metal plate and the surface of pure single crystals of ice, both before and after the ice was rubbed with another single crystal or with a plane. He found changes in the potential difference ranging up to 0.2–0.3 V after the rubbing. Unfortunately, he did not realize that he simply produced an ice–metal contact potential or, in other words, he measured a difference in electron work functions between the metal plate and the ice. The observed relaxation time was very long (hours at –10°C) and had nothing in common with the dielectric relaxation time in ice, which is $5 \times 10^{-5}$ seconds at that temperature. The effect that Takahashi found is likely ascribable to a difference in the structure and thickness of the surface charge double layer on fresh and aged ice surfaces. The layer slowly changed by adsorption of impurities from the air and diffusion of the impurities in ice. We will discuss such an electric double layer in the next section.

**Frictional electrification**

This writer (Petrenko and Colbeck 1995) studied frictional electrification on cylindrical samples of polycrystalline ice grown from very pure, deionized and degassed water. A polycrystalline ice layer, of about 2 cm thickness and a typical grain size of 5–12 mm, was frozen onto the outside of a stainless steel cylinder (Fig. 1). The cylinder was mounted on a lathe located inside a coldroom where temperature could be controlled within ±0.2°C. All ice samples were machined with a cutter to an outer diameter of 10 cm and then subsequently polished with sandpaper. The ice static conductivity $\sigma_s$ was $10^{-9}\ \Omega^{-1} m^{-1}$ at $T = -30°C$ and $10^{-7}\ \Omega^{-1} m^{-1}$ at $T = -10°C$. The measurements of $\sigma_s$ were made both with the apparatus at rest and during experiments. No difference was found among $\sigma_s$ values measured before, during and after the friction experiments. This showed that possible local melting and refreezing of the ice surface does not significantly change the ice conductivity. When the cylinder rotated, a frictional force changed the belt tension ($T_2 - T_1$). Then, the friction coefficient $\mu$ could be calculated as

$$\mu = \frac{1}{\alpha} \operatorname{arcth}\left\{\frac{T_2 - T_1}{T_1 + T_2}\right\} \tag{1}$$

where $\alpha$ is an angle shown in Figure 1.

A schematic of the experimental setup is shown in Figure 2. Reverse rotation of the cylinder allowed us to measure $T_2$ instead of $T_1$. Polyethylene, aluminum and stainless steel belts of 2.5-cm width were used as the sliders, and measurements were made at temperatures from –5 to –35°C and at sliding velocities from 0.5 to 8 m/s.

To determine whether friction causes melting, a thin thermocouple (0.1 mm) was attached to the outer



Figure 1. Ice friction and ice electrification measurements in the laboratory (top) and on snow in the field (bottom) (after Petrenko and Colbeck 1994).
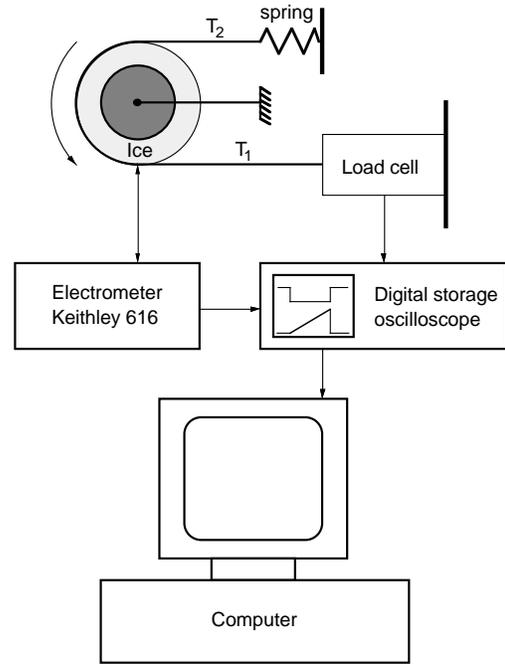


Figure 2. Experimental setup (after Petrenko and Colbeck 1994).

3
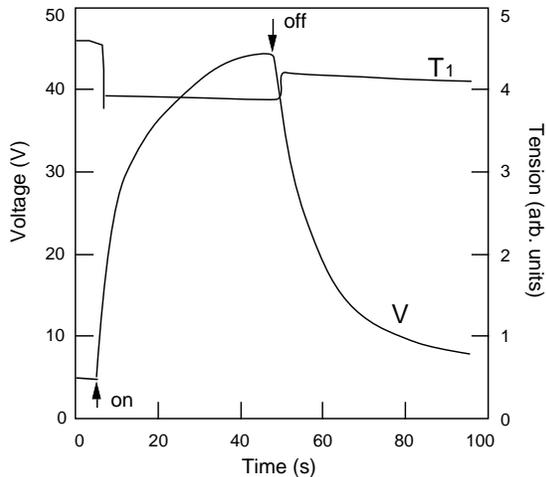
*Figure 3. Potential difference* V *across 75-µm-thick polyethylene film and its tension* T *(after Petrenko and Colbeck 1994). Sliding velocity was 1 m/s. The arrows indicate when the lathe was switched on and off. Temperature was –19°C.*
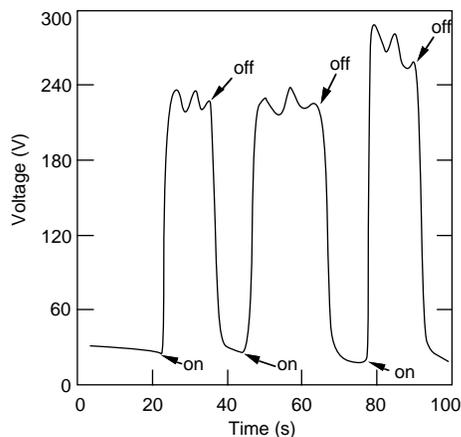


*Figure 4. Potential difference* V *between ice and a stainless foil. Sliding velocity was 1 m/s (after Petrenko and Colbeck 1994). Temperature is –30°C. The arrows indicate when the lathe was switched on and off.*
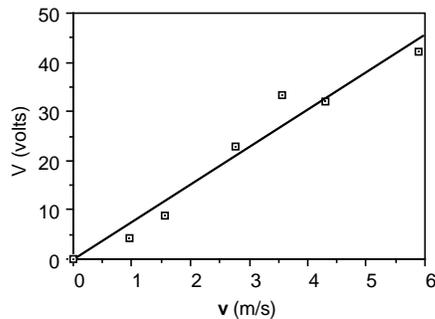


*Figure 5. Dependence of the potential difference between ice and stainless steel slider on sliding velocity (after Petrenko and Colbeck 1994).* T = –10°C.

side of the thin (75-µm) metal and dielectric belts sliding on the ice. The maximum heating by friction did not exceed 1°C; hence, general melting of the ice cylinder surface did not take place, although there may have been some local melting at a few points of direct ice–slider contact.

Significant frictional electrification was found for all sliding materials used (e.g., Fig. 3 and 4). The potential differences *V* observed were comparable both when the belt slid on its own circular track on the ice cylinder's surface and when it slid continuously on a fresh surface (spiral track). The electrification of the ice surface was not homogeneous. Normally, it was possible to find two positions along the 30-cm-long cylinder where *V* differed by a factor of two. Since the belt covered many ice grains, contributions from individual grains were not significant and added only a small oscillating component to *V*.

Typically, the potential differences generated between ice and metal were about 300 V (ice/Al, –31.5°C, 2 m/s). Under the same experimental conditions, the electrical field generated by the friction of ice on polyethylene reached $E = 2.1 \times 10^6$ V/m. This magnitude was calculated as the ratio of the potential difference across the film to the film thickness *L*. When the electrification was measured in the temperature interval from –4.5 to –35°C and for sliding velocities from 0.5 to 8 m/s, the sliders always received a positive charge. The electrification increased with decreasing temperature and increasing sliding velocity (Fig. 5). The maximum *V* = 1.6 kV was found at the lowest temperature *T* = –35°C and the highest sliding velocity *v* = 8 m/s.

From the measurements of a current *I* passing through the electrometer when it was used as a current meter, we found that the coupled ice–slider acted as a charge generator (Fig. 6). Moreover, at temperatures above approximately –12°C, the current is proportional
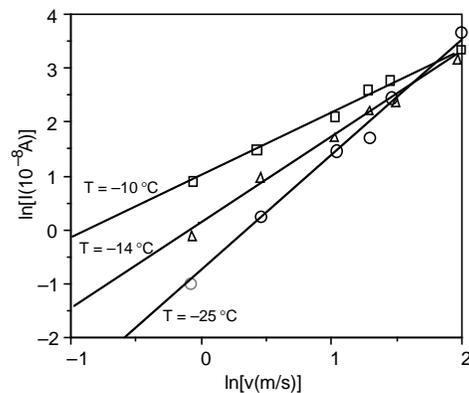


*Figure 6. Dependence of the electric current though ice/metal slider interface on sliding velocity at three different temperatures (after Petrenko and Colbeck 1994).*

4

to sliding velocity. Thus

$$I = \frac{dQ}{dt} = \lambda \frac{ds}{dt} \propto \boldsymbol{v} \qquad (2)$$

where $Q$ = electrical charge
  $\lambda$ = surface charge density that the slider picked up from the ice surface
  $s$ = area swept
  $\boldsymbol{v}$ = sliding velocity
  $t$ = time.

When the input impedance of a measuring device is much larger than the resistance of ice $R$, the charge generated flows through the ice, resulting in a potential difference $V$

$$V = IR . \qquad (3)$$

Since $R$ for ice increases exponentially with decreasing temperature (see the *Electrical Properties of Ice* [Petrenko 1993b]), the observed electrification rises rapidly at low temperatures. The charge density $\lambda$ found at $T = -10°C$ was about $1.6 \times 10^{-6}$ C/m$^2$ and $10^{-5}$ C/m$^2$ at $-35°C$. An even higher charge density of about $10^{-4}$ C/m$^2$ accumulated at the ice/dielectric slider interface. Since it is unlikely that a slider picks up all the surface charge from the ice, these values of $\lambda$ appear to be a lower limit.

At temperatures below $-10°C$, the density of charge collected from the surface becomes nonlinearly dependent on the sliding velocity (see Fig. 6). While at $T = -10°C$, $I$ is proportional to $\boldsymbol{v}$, at $-14°C$ $I$ increases as $\boldsymbol{v}^{1.5}$ and at $T = -25°C$ it increases as $\boldsymbol{v}^2$.

In the field experiments, we used an alpine ski as a slider on snow (Fig. 1). The ski itself acted as a flat capacitor $C_0$ to measure an electrical field of strength $E$ generated by charge density $\lambda_{ski}$ that accumulated on the bottom ski surface. A larger capacitor $C = 2 \mu F$, connected in parallel with $C_0$, reduced the potential difference $V$ to a magnitude that could be measured by a portable data logger carried by the skier in a backpack. It is easy to show that

$$V = \frac{\lambda_{ski} d}{2\varepsilon_0 \varepsilon} \frac{C_0}{C + C_0} \qquad (4)$$

where $\varepsilon_0$ and $\varepsilon$ are the dielectric permittivities of a vacuum and of the material between the metal plates in the ski respectively. The reduction factor $C_0/(C + C_0)$ was $5.1 \times 10^{-4}$.

The field measurements of snow frictional electrification were made in deep powder snow in British Columbia. Figure 7 shows a typical record of $V$ taken at $-4°C$ at three different velocities. The general char-
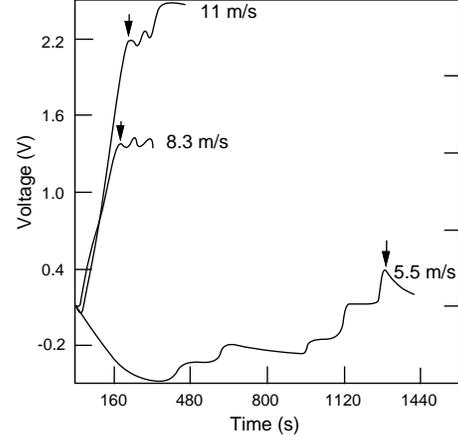


*Figure 7. Records of the potential difference* V *across a capacitor built into a ski at three sliding velocities (after Petrenko and Colbeck 1994). Temperature was $-4°C$. Skier started at* t = 0 *and slowed at the moments marked with the arrows.*

acter of the electrification observed in the field experiments agrees well with the laboratory results. One of the most noticeable differences is that, in the field, $V$ first becomes negative and only then positive. At the highest speed, $V$ reached 2.2 V, which corresponds to $\lambda = 3.6 \times 10^{-7}$ C/m$^2$. This charge density was comparable with a value of $1.6 \times 10^{-6}$ C/m$^2$ found on ice. In the absence of the buffer capacitor $C$, $V$ would have been $4.4 \times 10^3$ V if there had been no electrical breakdown of the air or the ski dielectric material. And this is not yet at saturation. According to the laboratory results, we can expect even higher voltages at lower temperatures. A reader interested in ski electrification can find more details in Colbeck's (1994) publication.

Possible reasons for electrification by friction, i.e., the accumulation of the electrical charges transferred from the ice surface onto the slider, can be classified into two categories:

1. The slider sweeps up the charge already present at the ice surface.

2. Friction somehow produces a spatial separation of the charge, which is then swept up by the slider.

After analyzing our data and the known ice surface properties, we favor mechanism 1. Figure 8 shows a very general electrical charge distribution in ice near the surface. In a thin subsurface layer, a charge layer of an extremely high density $\lambda_s$ is formed. The major factor leading to its formation is the ordering of dipole moments of the water molecules in the upper monomolecular layer, resulting in polarization $P_0$. Such ordering was initially suggested by Weyl (1951) for water and was later used by Fletcher in his model of the ice surface structure. Other evidence for the existence of such an ordered layer of water molecules at the
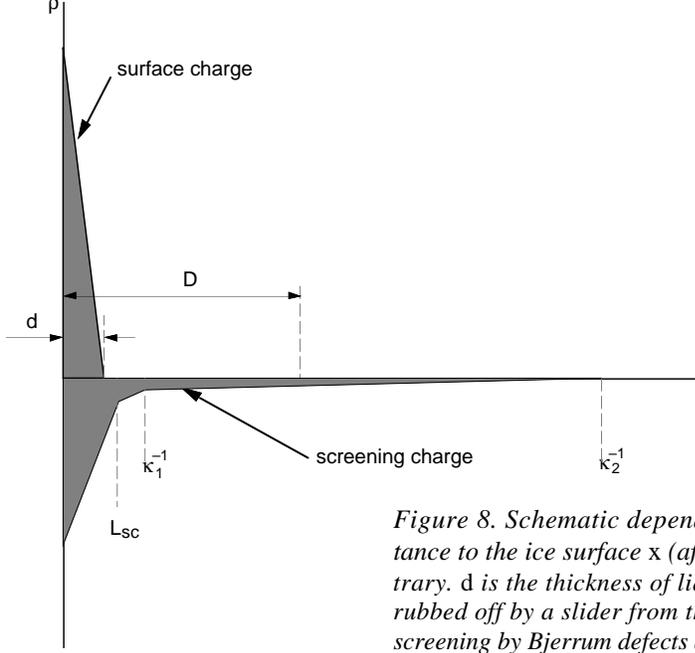
*Figure 8. Schematic dependence of the space charge density ρ on the distance to the ice surface* x *(after Petrenko and Colbeck 1994). Scales are arbitrary.* d *is the thickness of liquid-like layer,* D *is the thickness of the ice layer rubbed off by a slider from the ice surface, and* $\kappa_1^{-1}$ *and* $\kappa_2^{-1}$ *are the length of screening by Bjerrum defects and ions correspondingly.*

ice surface comes from the high adsorption coefficient of ice at temperatures above $-40°C$ (Ocampo and Klinger 1983), and the results of computer simulations carried out by Bush and Devlin (1991). At the same time the polarization of water molecules in the bulk is zero. Therefore, the polarization $\vec{P}$ drops from $\vec{P}_0$ at the surface ($x = 0$) to 0 ($x = \infty$). This nonuniform polarization results in a surface charge of a high density

$$\lambda_s = -\int_0^\infty \frac{\partial P}{\partial x} dx = P_0. \tag{5}$$

An estimation using eq 5 gives $\lambda_s \approx 2 \times 10^{-1}$ C/m$^2$. Other possible reasons accounting for the formation of $\lambda_s$ could be adsorption of ions from the air and the presence of the surface electronic states.

In thermal equilibrium the surface charge $\lambda_s$ must be neutralized by the opposite screening charge $\lambda_{sc}$, equal to the former in magnitude, which is distributed, however, in a much thicker screening layer. The screening of the surface charge in ice was considered in Petrenko and Ryzhkin (1984a), and in Petrenko and Maeno (1987). The screening charge is composed of protonic charge carriers (Bjerrum D- and L-defects and $H_3O^+$ and $OH^-$ ions). There are two screening lengths in ice $\kappa_1^{-1}$ and $\kappa_2^{-1}$

$$\frac{1}{\kappa_1} \cong \left[ \frac{e_3^2 (n_{30} + n_{40})}{\varepsilon_0 \varepsilon_\infty k_B T} \right]^{-\frac{1}{2}} \tag{6}$$

$$\frac{1}{\kappa_2} \cong \left[ \frac{e^2 (n_{10} + n_{20})}{k_B T \varepsilon_0 \varepsilon_s} \right]^{-\frac{1}{2}} \tag{7}$$

where $\varepsilon_0 =$ dielectric permittivity of vacuum
$\varepsilon_\infty = 3.2$, the high-frequency permittivity of ice
$\varepsilon_s \approx 100 =$ static dielectric permittivity of ice
$k_B =$ Boltzmann constant
$e_3 = 0.38e =$ charge of Bjerrum defects
$n_{10} =$ concentrations of $H_3O^+$ ions
$n_{20} =$ concentrations of $OH^-$ ions
$n_{30} =$ concentrations of D-defects
$n_{40} =$ concentrations of L-defects.

At the screening length $\kappa_1^{-1}$, which is determined by the concentration of majority carriers ($n_{30} + n_{40}$) and coincides with the well-known expression for the Debye screening length $\kappa_1^{-1}$, the field drops down from the original value $\lambda_s/\varepsilon_0\varepsilon_\infty$ to $\lambda_s/\varepsilon_0\varepsilon_S$. As we have seen, $\varepsilon_S \approx 10^2$, that is, $\kappa_1^{-1}$ is a characteristic length at which $\varepsilon_S$ attains a steady-state value. At larger $x$ the field drops down to zero because of screening by minority charge carriers, i.e., ions with a larger characteristic screening length $\kappa_2^{-1}$ determined by ion concentrations ($n_{10} + n_{20}$). Substitution of charge carrier concentrations in pure ice (Petrenko 1993b) into eq 7 and 8 gives at $T = -5°C$

$$\frac{1}{\kappa_1} \cong 3.4 \times 10^{-8} \, \text{m} \tag{8}$$

$$\frac{1}{\kappa_2} \cong 3 \times 10^{-5} \, \text{m}. \tag{9}$$

6

But at –35°C they are longer than eq 8 and 9 predict owing to the exponential dependencies of the charge carrier concentrations on temperature. At –35°C

$$\frac{1}{\kappa_1} \cong 8 \times 10^{-8}\,\mathrm{m} \tag{10}$$

$$\frac{1}{\kappa_2} \cong 1.6 \times 10^{-4}\,\mathrm{m}. \tag{11}$$

Notice that both the liquid-like layer and the principal screening length $\kappa_1^{-1}$ are very small. That makes it likely that a slider, when rubbing ice, sweeps off the surface charge together with the most of the screening charge. That leaves just a small fraction of all $\lambda_s$ on the ice surface (see Fig. 8). This may explain why the density of the surface charge taken away by the sliders ($\lambda \leq 10^{-5}$ C/m$^2$) was much smaller than the theoretically predicted $\lambda_s \approx 2 \times 10^{-1}$ C/m$^2$. Another factor decreasing $\lambda$ is that the real contact area is much smaller than the slider surface, and hence the slider does not sweep off the whole area of the interface as assumed in eq 2.

The described mechanism of electrification by friction, thus, though hypothetical, is based on firm and clear deductions from the surface physics of ice and can be tested experimentally in the future, since it implies characteristic dependencies on temperature, sliding velocity, thickness of the "erased" layer and doping of ice.

Other mechanisms that may in principle contribute to the frictional electrification of ice are the motion of charged dislocations during the plastic deformation of ice subsurface regions (Takahashi 1969a, Petrenko and Whitworth 1983), a charge separation by microcracks in ice during cleavage of surface layers (Petrenko 1993a) and the Workman-Reynolds (1949, 1950) effect (charge separation during refreezing of ice). It is unlikely that any of these phenomena is able to account for the large magnitude of the potential difference, 1.6 kV, observed in our research. Under the most favorable conditions, the first two mechanisms generated $V$ values that are much less then 1 V and the Workman-Reynolds effect generated about 100 V. Also, the Workman-Reynolds effect reaches a maximum in doped ice samples while frictional electrification decreases with doping. As discussed in the previous section, the thermoelectric effect can add only a negligible contribution.

The fact that at higher temperatures (–5 to –10°C) the electrification is proportional to the sliding velocity ($V \propto v$) while at lower temperatures ($\leq$ –25°C) $V$ is proportional to $v^2$ can be explained in terms of the length of the electrically charged track on the ice surface $L_t$ that a slider leaves behind. When the slider is moving at constant velocity, any electrical charge picked by it has to relax, flowing over the distance $L_t$ to the location of the opposite electrical charge behind the slider. Then the resistance $R$ in eq 3 is proportional to $L_t = \tau_D \cdot v$ and $V$ is proportional to $v^2$. ($\tau_D$ is the Debye relaxation time of the ice.) Measurements of $\tau_D$ revealed that $L_t \approx 0.1$ mm at –5°C but $L_t \approx 1$ cm at –35°C. Hence, at the high temperature the discharge takes place locally under the slider since $L_t$ is much less than the slider dimensions (2.5 cm). In that case $R$ does not depend on $v$ and $V \propto v$. But when at the low temperatures, $L_t$ becomes comparable with the slider dimensions, and $R \propto L_t \propto v$ and $V \propto v^2$.

**Effect of electrical fields on ice friction**

Earlier (Petrenko 1994a), it was demonstrated that the application of an external dc bias to the ice/slider interface can double the force of dynamic and static friction between ice and metals and between ice and dielectrics. The experimental techniques, the ice samples and experimental conditions used were similar to the ones described in the previous section (see Fig. 1 and 2). The measurements were performed at temperature intervals from –5 to –30°C, with sliding velocities from 0.5 to 8 m/s and the dc bias within the range from –3 to 3 kV. All slider materials created a strong increase in apparent friction coefficient when the bias $|V| \geq 1$ kV was applied. Owing to the high dc impedance of pure ice, the electrical power consumed from the power supply was very small (about $10^{-3}$ W at –30°C for metal sliders and even less for dielectric ones).

Figure 9 depicts the changes in polyethylene belt tension $T_2$ when a 3-kV bias was applied to the ice cylinder and the foil electrode attached to the outer surface
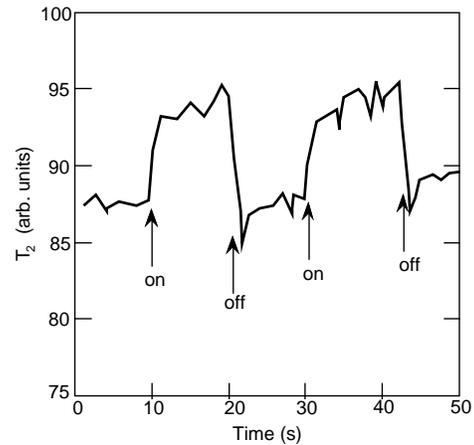


*Figure 9. Changes in tension of the polyethylene belt ($T_2$) when a 3-kV bias is switched on and off (after Petrenko 1994a). Temperature is –30°C. Sliding velocity is 2 m/s. The friction coefficient $\mu \approx 0.3$ at $V = 0$ and $\mu \approx 0.5$ at $V = 3$ kV.*

of the dielectric film, as shown in Figure 1. In a static electrical field, ice behaves as a conductor so that the entire bias is applied across the dielectric belt and the air gap between the belt and the ice cylinder. Since $T_2$ increases when frictional force increases, the effect shown in Figure 9 corresponds to greater friction with the applied voltage. Within the limits of experimental error ($\pm 20\%$, determined by oscillations of $T_2$), there was no difference in the effects of positive and negative biases on the apparent ice friction coefficient $\mu$. At higher temperatures (from $-5$ to about $-10^\circ$C), ($T_2 - T_1$) becomes comparable with oscillations in the belt tension because of the small magnitude of ice friction. This results in the fact that while the effect of a dc bias is noticeable at these temperatures, it becomes much more pronounced only when the temperature decreases.

The change in the frictional force can be explained by means of electrostatic pressure $P_{el}$, which increases the normal pressure of the belt on ice

$$P_{el} = \frac{\varepsilon_0 E^2}{2} = \frac{\varepsilon_0 V^2}{2L^2} \tag{12}$$

where  $V$ = applied voltage
  $E$ = electrical field strength at the ice/slider interface
  $\varepsilon_0$ = dielectric permittivity of a vacuum
  $L$ = thickness of the belt.

$P_{el}$ reaches a maximum in the absence of an air gap between the ice and the slider. In this case and under conditions indicated in Figure 9, $P_{el} = 4$ kPa, which exceeds the average normal pressure $P_0$ of the belt on ice by a factor of four. Under the experimental conditions described, we can expect a fivefold increase in the apparent friction coefficient. Since we see a smaller effect, we assume that there was an average (and dynamic) air gap between the ice and the slider of about 0.2 mm, sufficient to reduce the effect on the observed

magnitude. Also, $P_{el}$ should not depend upon the bias polarity, in agreement with the experimental results.

When metallic belts made of aluminum or stainless steel foils were used, the effect of dc bias on friction was comparable to the results obtained with dielectric sliders (see Fig. 10). In this case the dc bias was applied across the entire thickness of the ice between the central metal cylinder and a metal slider. The effects of positive and negative bias on friction were similar to each other but not quite reversible. Namely, when the bias was switched off, it took a long time (several minutes at $-30^\circ$C) to restore the initial frictional force. Since the electrical field vanishes during the much shorter time of about 0.1 second (this was a time constant of the electrical circuit used), the observed effect of the electrical field on ice–metal friction cannot be explained in terms of electrostatic pressure. However, even more serious evidence in favor of disregarding the importance of electrostatic pressure comes from a quantitative comparison of $P_{el}$ and $P_0$. While $P_0$ remained the same, as in experiments with dielectric sliders (about 1 kPa), $P_{el}$ has not exceeded 0.18 Pa (see eq 12). This smaller electrostatic pressure comes from a larger $L$, across which the dc bias $V$ was applied. In this case $L$ was equal to the ice thickness (1.5 cm) since the central metal cylinder and the metal belt acted as two electrodes attached to a poor conductor (ice). The absence of any sizable potential drop at the ice/metal interfaces was proven by perfectly linear current voltage characteristics. The field effect was more pronounced at low temperatures for the same reason as in the case of the dielectric sliders, that is better signal-to-noise ratio.

The application of electrical fields also increased static friction between ice and metals (see Fig. 11). This phenomenon was very noticeable at temperatures above $-15^\circ$C, at which it takes just a few seconds for a metal belt to freeze to the ice cylinder. At lower temperatures, when a slider rested just few seconds be-
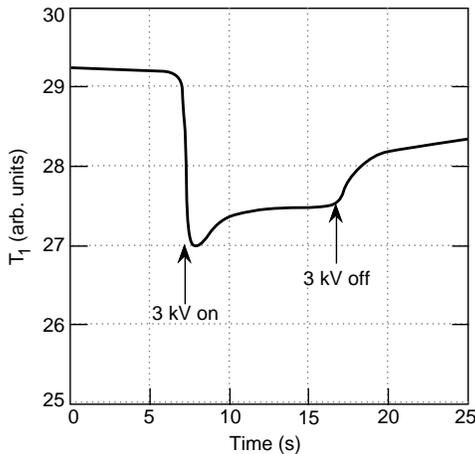


*Figure 10. Changes in tension of the aluminum belt* ($T_1$) *when a 3-kV bias is switched on and off (after Petrenko 1994a). The smaller* $T_1$ *is, the larger friction is (see Fig. 1). Temperature is $-30^\circ$C. Sliding velocity is 2 m/s. The friction coefficient $\mu \approx 0.34$ at* V = *0 and $\mu \approx 0.47$ immediately after* V = *3 kV is turned on.*

*Figure 11. Changes in tension of the stainless steel foil belt when the ice cylinder direction of rotation reverses (after Petrenko 1994a). Temperature is –10°C. Peaks correspond to static friction. The two sets of dashed lines indicate the average magnitude of the belt tension $T_1$ and $T_2$ when 2-kV dc bias between ice and steel was "on." The static friction coefficient $\mu \approx 0.267$ at V = 0 and $\mu \approx 0.312$ at V = 2 kV.*
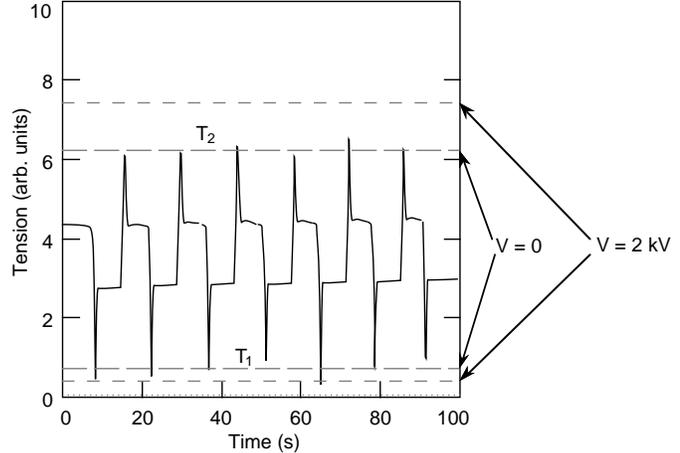
tween sliding, there was usually no pronounced difference between static and dynamic friction, and the electrical field affected friction in the manner shown in Figure 10. Once again, a strong field effect such as that shown in Figure 11 cannot be explained in terms of electrostatic pressure.

As working hypotheses accounting for the phenomena observed, I considered electrostatic pressure (see eq 12), the effect of static electrical fields on the plastic deformation of ice and expansion of the contact area caused by electrical fields.

Electrostatic fields externally applied to the interface between ice and a dielectric slider are able to significantly alter normal pressure and, consequently, the friction force (eq 12). Perhaps a more important and interesting fact is that such electrostatic attraction between ice and a slider always occurs by itself owing to the frictional electrification. Under certain conditions, such electrification can contribute to the formation of the friction force.

The effect of electrical fields on plastic deformation of thin ice monocrystals (Petrenko and Schulson 1993) was used to explain the action of an external electrical field on the dynamic friction of metal sliders against ice. It appears that an application of relatively small dc electrical biases, on the order of 50 V, to an ice/metal interface reduces by nearly an order of magnitude the plasticity of a layer of ice of 50–100 $\mu$m thickness adjacent to the metal. This in turn is caused by the extraction of the major charge carriers (Bjerrum defects) from the region near the electrode by the electrical field (Petrenko and Schulson 1992). Depletion of Bjerrum defects from the subsurface layer of ice alters the conditions of dislocation motion, which results in the reduction of plasticity. When ice slides, there is a plastic shear deformation in the contact zones between the ice and slider. Therefore, a reduction in the plasticity of ice when a voltage V is applied results in an increase

of resistance to shear stress, or in other words results in an increase of frictional force.

The effect of an electrical field on the plasticity of ice may also contribute to the observed effect of a field on static friction (see Fig. 11). In addition to that mechanism, there is the possibility that the applied field changes the contact area between the ice and metal. The following grounds support this assumption: the effect of an electrical field on static friction was observed only when the temperature was high enough that a quasi-liquid film, characterized by low viscosity and a large self-diffusion coefficient as compared to ice, existed at the ice surface. When a strong electrical field is present in the voids between ice and metal, ice is attracted into these regions by the electrostatic pressure and tends to fill them. Since the static dielectric permittivity of ice is quite large ($\varepsilon_s \approx 100$), the driving force of electrostatic pressure is also quite large

$$P = \frac{\varepsilon_0(\varepsilon_s - 1)E^2}{2}. \tag{13}$$

A mass transfer at high temperatures can efficiently occur along the quasi-liquid film, filling air gaps between the ice and the metal slider and increasing the ice adhesion.

The above experimental facts and discussion show the importance of electrical effects on ice friction. Physical mechanisms of the phenomena are not determined yet. We have considered here only a few obvious mechanisms that are known to be applicable under similar experimental conditions and can be easily estimated. Other mechanisms, such as electrolytic effects caused at the metal/ice interface, the role of thin local liquid patches, modification of the mechanical properties of ice surface by multiple local melt–refreeze, etc., should also be analyzed. This is an extensive field for future study.

## ELECTRO-ELASTIC EFFECTS

### Is ordinary ice $I_h$ piezoelectric?

Perhaps the most well-known electromechanical phenomenon is piezoelectricity. Application of *uniform* elastic strain to a piezoelectric crystal causes its electrical polarization. The electrical polarization is characterized by a vector $\vec{P}$. Crystalline quartz is a well known example of a piezoelectric material. Mathematically, the direct piezoelectric effect is described

$$P_i = \varepsilon_0 \chi_{ij} E_j + e_{ijk} \times \varepsilon_{jk} \qquad (14)$$

where $P_i = i^{th}$ component of the polarization vector
$\quad e_{ijk}$ = piezoelectric stress tensor
$\quad \chi_{ij}$ = electrical susceptibility tensor
$\quad \varepsilon_{jk}$ = strain tensor.

The inverse effect produces a contribution to the strain

$$\varepsilon_{mn} = c_{mnij}\sigma_{ij} + d_{kmn} E_k \qquad (15)$$

where $c_{mnij}$ = stiffness tensor
$\quad \sigma_{ij}$ = stress tensor
$\quad d_{kmn}$ = piezoelectric strain tensor.

Two piezoelectric tensors relate

$$d_{kmn} = s_{mnij} e_{kij} \qquad (16)$$

where $s_{mnij}$ is the compliance tensor.

The physical mechanism of piezoelectric polarization is very simple and can be explained in the following way. The atomic structure of all piezoelectric crystals may be thought of as consisting of pairs of positive and negative ions. Since one such pair makes an electric dipole, we can say that the whole structure of a piezoelectric crystal is composed of such elementary dipoles. Now, using this simplified interpretation of piezoelectric polarization, we can easily estimate its absolute magnitude, which can later be compared with the magnitude of pseudo-piezoelectric effects in ice. Let us take a typical length of an elementary dipole $a = 10^{-10}$ m and the dipole concentration $N = 3 \times 10^{28}$ m. Then

$$P \approx \frac{Nae}{\varepsilon_0 \varepsilon} \approx 2 \times 10^{10} \, \text{C/m}^2. \qquad (17)$$

Application of a strain $\varepsilon_{ii}$ varies the length $a$ by the factor of $\varepsilon_{ii}$. The piezoelectric polarization is described with the change in the polarization vector

$$\Delta P \approx \varepsilon_{ii} P. \qquad (18)$$

Hence, the components $e_{ijk}$ of the piezoelectric

stress tensor in eq 14 should be of the order of $P$

$$e_{ijk} \approx P \approx 2 \times 10^{10} \, \text{C/m}^2. \qquad (19)$$

The reader can check that eq 19 gives the correct order of magnitude for strong piezoelectric crystals such as segnet salt ($4.2 \times 10^{10} \, \text{C/m}^2$). In quartz, which is a weak piezoelectric, $e_{ijk}$ is about $1.5 \times 10^9 \, \text{C/m}^2$.

Figure 12 illustrates generation of the electrical polarization $\vec{P}$ under the action of uniform compression. Looking at the figure, we can easily realize that the piezoelectric effect is incompatible with a center of symmetry. Otherwise, the vector $\vec{P}$ would not know which direction to go: to the left or to the right. According to Neumann's principle, the symmetry of any physical property of a crystal cannot be less than the symmetry in the atomic structure of that crystal. In our case this means that crystals with a center of symmetry in the atomic structure cannot exhibit a piezoelectric effect.
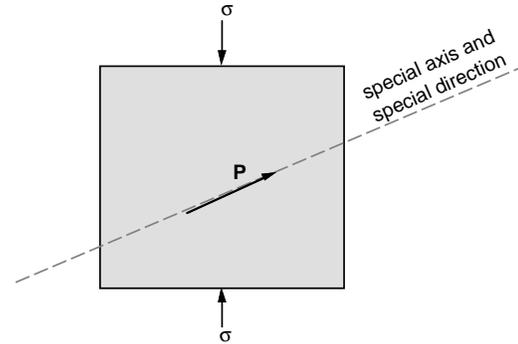


*Figure 12. Generation of piezoelectric polarization in a crystal under the action of the uniform, uniaxial compression.*

Let us apply Neumann's principle to ice. Ice is a molecular crystal consisting of water molecules. While the centers of the water molecules are arranged into a regular wurtzite lattice, the molecular dipoles may have one of six allowed orientations and are not ordered (see Hobbs 1974 and Petrenko 1993c). Such a random orientation of the dipoles results in zero polarization of ice as it is shown in Figure 13b. In other words, ice has a kind of statistical center of symmetry. An application of uniform strain, as shown in Figure 13c, may cause some reorientation of a small fraction of the molecules but without distortion of the center of the symmetry (Petrenko and Ryzhkin 1984b). The reorientation of water molecules in ice under strain is responsible for the ice anelastic relaxation. We can conclude now with confidence that ordinary ice $I_h$ cannot be an ordinary piezoelectric. Though some early papers reported observation of a piezoelectric effect in ice (see, for instance, Rossman 1950), it is likely that this resulted

*a. Electric dipole moment of a water molecule.*

*b. Chaotic orientations of water molecules in ice before stress.*

*c. Partial ordering of the water molecules in ice after stress was applied.*
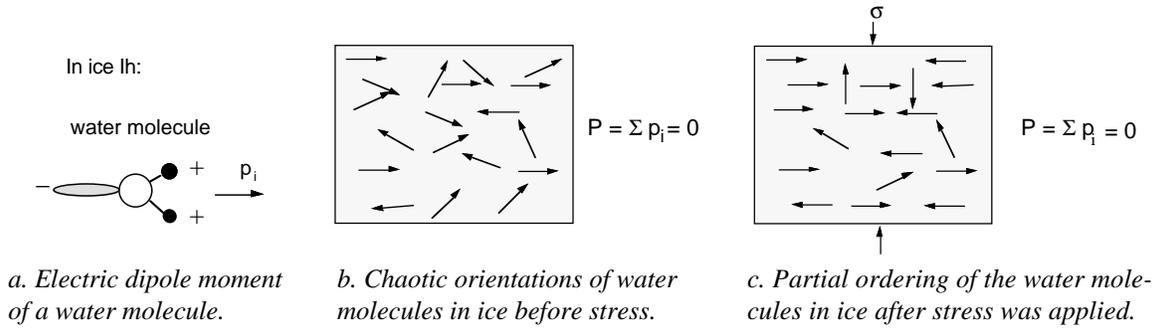
*Figure 13. Application of Neumann's principle to ice.*

from some of the pseudo-piezoelectric effects discussed later in this report.

**Phonon-induced polarization of ice**

Whalley and Klug (1984) noticed that while a macroscopic bulk of ice does not have a dipole moment, at the microscopic scale of about of tens of angstroms, the ice lattice may be polarized by statistical fluctuations in the small statistical ensembles. That means that at the microscopic scale ice can behave as a piezoelectric. As Whalley and Klug showed, this can affect propagation of elastic waves with a wavelength comparable to the size of the polarized micro-regions. The same phenomenon should also result in additional absorption of infrared light.

**Polarization induced by nonuniform strain**

Though ordinary ice $I_h$ is not a conventional piezoelectric, under some special conditions elastic strain can induce an electrical polarization in it. Such special conditions are gradients of strain, temperature or impurity concentration and also an externally applied electrical field. All these factors destroy the statistical center of the symmetry, whose existence imposes a ban on the conventional piezoelectricity of ice.

Let us start the consideration of such pseudo-piezoelectricity from an electrical polarization of ice caused by nonuniform strain. This phenomenon was first observed by Evtushenko et al. (1984), who have studied electrical fields generated by bending vibrations in thin pure single crystals of ice. Later (Evtushenko et al. 1987, Evtushenko and Petrenko 1991) such polarization was measured in a wide temperature range, from 0 to –80°C, on ice doped with HF, HCl and $NH_3$. The wide temperature range and the doping were used to study the phenomenon of ice having different types of majority charge carriers. Also, a theoretical model of the pseudo-piezoelectric effect was developed, which is explained below.

It was suggested that in ice under a nonuniform strain, protonic charge carriers migrate along the pres-

sure gradient in the same way as an air bubble moves upwards in water (Fig. 14). The reason for such migration of the defects is that their specific volume differs from that of a water molecule. As the result, point defects larger then a water molecule will migrate in the direction opposite to the pressure gradient, while those with a smaller specific volume will migrate in the direction of the gradient. Some important practical cases in which nonuniform strain causes the protonic defect's migration and an associated electrical polarization are shown in Figure 15. Also, since there is an oscillating gradient of pressure in a longitudinal wave, such a wave is followed by a wave of weak electrical polarization in ice.

The formation of any protonic point defect results in deformation of the surrounding lattice. In the case of Bjerrum defects, the defective hydrogen bonds are weaker than the normal ones, and therefore they will be longer. This is obvious in particular for a D-defect, where there exists an extremely strong repulsion between two protons on one hydrogen bond. Accordingly, we can assume that Bjerrum defects "expand" ice, increasing its volume. If ice is under pressure $P$, then the formation energy of the $i^{th}$ defect $E_{ai}$ is increased by the
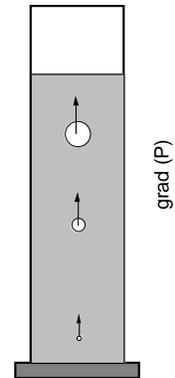


*Figure 14. Air bubble migration against a pressure gradient in water.*

*a. Indentation.*    *b. Crack.*    *c. Bend.*
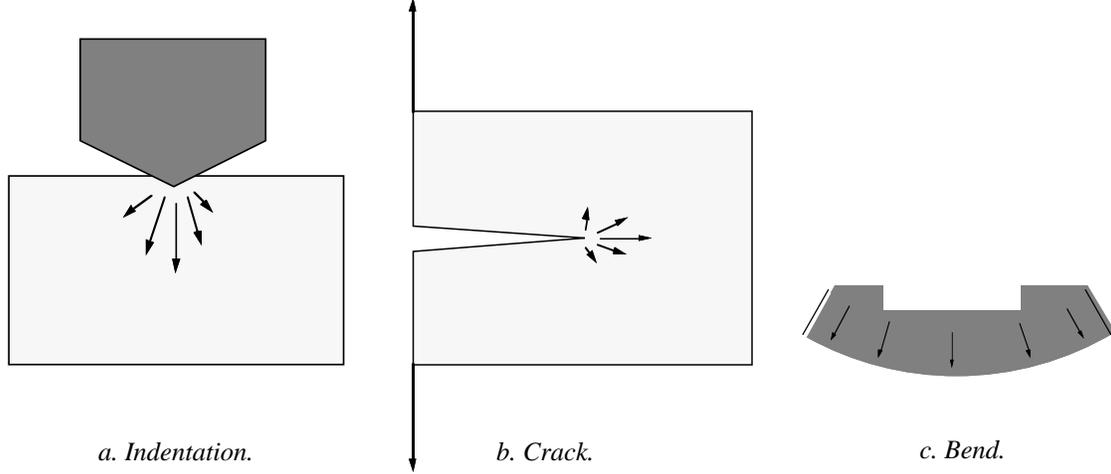
*Figure 15. Some practical cases in which nonuniform strain generates electric polarization of ice. The arrows indicate the direction of motion of charge carriers.*

amount of work against this pressure

$$E_{ai}(P) = E_{ai}(0) + P\gamma_{ai} \tag{20}$$

where $\gamma_{ai}$ is the so-called activation volume.* For the defects that increase volume, $\gamma_{ai}$ is positive, and their formation energy is raised proportionally to the applied pressure. This results in an exponentially decreasing concentration of such defects with increasing pressure. Since the formation energy of defects $E_{ai}$ depends on the applied pressure $P$ according to eq 20, in the presence of a pressure gradient, there is a force $\vec{F_i}$ acting upon the defects

$$\vec{F_i} = -\text{grad}(E_{ai}) = -\gamma_{ai}\ \text{grad}(P). \tag{21}$$

To find a resulting flux of the defects $\vec{j_i}$, we have to add this force to the transport equation

$$\vec{j_i} = \left(e_i\vec{E} - \eta_i\Phi\vec{\Omega}\right)n_i\mu_i - D_i\ \text{grad}\,n_i \tag{22}$$

where  $e_i$ = electric charge of the defects
$E$ = electric field strength
$n_i$ = defect concentration
$\mu_i$ = defect mobility
$D_i$ = defect diffusion coefficient
$\vec{\Omega}$ = configuration vector

---

* Normally, in solids pressure is not hydrostatic, i.e., $\sigma_{11} \neq \sigma_{22} \neq \sigma_{33}$. Then, instead of eq 20 we should use

$$E_{ai}(\sigma_{ij}) = E_{ai}(0) + \gamma_{ai}(\sigma_{11} + \sigma_{22} + \sigma_{33}) = E_{ai}(0) + \gamma_{ai}\sigma_{jj} \tag{20a}$$

or

$$E_{ai}(\varepsilon_{ij}) = E_{ai}(0) + \alpha_{ai}\varepsilon_{jj} \tag{20b}$$

where $\alpha_{ai}$ is a deformation-potential constant of $i$th type charge carrier.

$$\vec{\Omega} = \int_0^t \left(\vec{j_1} - \vec{j_2} - \vec{j_3} + \vec{j_4}\right)dt. \tag{23}$$

The quantities $\eta_i$ are given by

$$\eta_i = 1,-1,-1,1 \qquad \text{for } i = 1,2,3,4 \tag{24}$$

and

$$\frac{\Phi}{T} = 3.85k_B r_{oo} \tag{25}$$

where $r_{oo} = 2.76$ Å is the oxygen–oxygen distance in ice (Jaccard 1964). To find the electrical field strength caused by the pressure gradient $\nabla P$, we should solve the system of eq 22–23 under particular initial and boundary conditions. Thus, in the case of one dominating carrier type and static $\nabla P$

$$\vec{E} = \frac{\gamma_{ai}\nabla P}{e_i + \dfrac{\varepsilon_\infty\varepsilon_0}{e_i}\cdot\Phi} \tag{26}$$

while for two types of charge carriers, for example $H_3O^+$ ions and L-defects, and static pressure gradient the electrical field is

$$\vec{E} = \frac{(\gamma_{a4} - \gamma_{a1})\nabla P}{e} \tag{27}$$

(see Evtushenko et al. [1987] and Evtushenko and Petrenko [1991]). Electrical polarization of ice caused by stable and growing cracks was calculated in another publication (Petrenko 1993a). Electromagnetic emission generated by such cracks will be described in the section on electro-fracture effects.

Equations 26–27 show how the defect's activation volumes can be determined from measurements of the

12

pseudo-piezoelectric effect. Indeed, that method was used (Evtushenko and Petrenko 1991) to determine $\gamma_{ai}$. By varying temperature and doping, we determined activation volumes of all four types of protonic defects in ice. Figure 16 shows time dependencies of an electrical bias generated across a thin ice sample when a step-shaped pulse of bending was applied to the sample. The ice was doped with $NH_3$ in such concentration that D-defects were majority charge carriers above –30°C, but below –35°C $OH^-$ ions dominated. The observed decay of the signals is mainly attributable to a final input impedance of the measuring circuit used. Since the electrical charges of $OH^-$ ions and D-defects are opposite, so are the electrical biases caused by their migration.
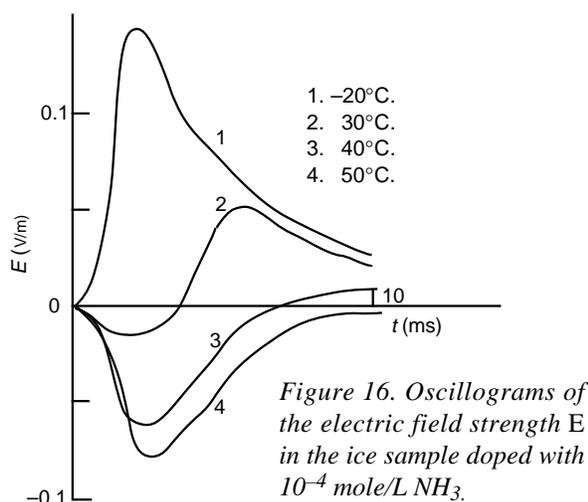


Figure 16. Oscillograms of the electric field strength E in the ice sample doped with $10^{-4}$ mole/L $NH_3$.

**Other pseudo-piezoelectric effects**

There are more trivial pseudo-piezoelectric effects. They can be observed when ice is already electrically polarized for some reason. For example, because of the thermoelectric effect (Brook 1958), ice is always polarized when there is a temperature gradient in it. The electrical potential difference generated is usually small since the thermoelectrical power of ice is low

$$\frac{\Delta V}{\Delta T} = \pm(2-4)\text{mV/°C} \qquad (28)$$

(see Bryant and Fletcher 1965, Takahashi 1966). More pronounced electrical polarization of ice can be induced by nonuniform distribution of impurity ions in ice. In this case $\Delta V$ can reach hundreds of millivolts and even 1 V (Brook 1958, Petrenko 1992a). Hence, we can say that a piece of ice acquires an electrical polarization if there are either temperature or impurity gradients in it. Elastic strain $\varepsilon_{ij}$ (even uniform) changes the dimensions of the ice sample, changing its dipole moment. When a characteristic frequency of applied

strain $\omega >> \omega_D$, where $\omega_D$ is a Debye frequency, the charge carriers in ice have no time to get redistributed in the bulk of the deformed ice and, in the first approximation, the oscillating part of the polarization $\approx \varepsilon_{ij}p$. At the lower frequencies $\omega = \leq \omega_D$, we have to allow for the ac bias arising at the elastic oscillations being applied to the bulk of ice, whose electrical conductivity and dielectric permittivity have a complicated frequency dependence (Hobbs 1974, Petrenko 1993b). Such electrical polarization induced by elastic strain in ice with temperature or impurity gradients, or both, was reported by Evtushenko et al. (1987).

## ELECTROMAGNETIC PHENOMENA IN ICE FRACTURE

At present we know of several electromagnetic phenomena that are associated with the presence or appearance of cracks in ice. They are electromagnetic emissions (EME) from growing cracks and stable cracks under varying stress, and also crack-induced changes in electrical conductivity and apparent dielectric permittivity of ice.

The most interesting and intriguing of these phenomena, EME from cracks, was primarily found under poorly controlled field conditions when a low signal-to-noise ratio left doubts and uncertainty about the phenomenon's existence. Later, EME from cracks in ice were reproduced and studied in a well-controlled laboratory environment. The laboratory results made it possible to develop physical models that explained that electromechanical effect. When the researchers were equipped with these models, they succeeded in obtaining reliable and well-reproducible detection of EME from cracking in lake and sea ice. At the present time, the EMP described below in this section are well understood and have even been found useful, both in ice mechanics and remote sensing of stress in ice. That is why we first start with a theoretical consideration of the physical processes that cause EME from cracks in ice and other associated phenomena. Then, we will discuss laboratory and field data and their interpretations.

### Theory

*Cracks splitting pre-polarized ice*

The main cause of EME from cracks in natural ice is the so-called "frozen-in" or "intrinsic" electrical field that is always presents in both sea and freshwater ice. This electrical field is generated by spatial nonuniformity in the concentration of ions dissolved in the ice bulk (Petrenko 1992a, 1994b). Figure 17 shows schematically such an electrical field inside granular ice. The electrical field originates from the nonuniform
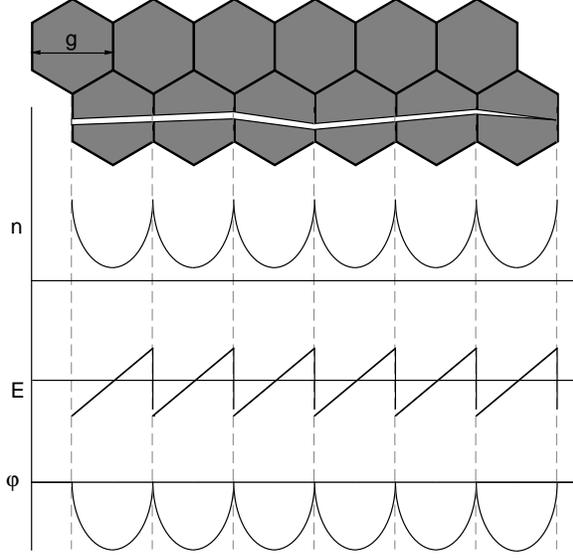
*Figure 17. Schematical representation of variations in ions' concentration* n, *electric field strength* E *and electric potential* φ *along the crack surface in granular ice.*

distribution of impurities in ice. Namely, when ice grains grow, impurities are pushed out by the phase boundary from grain centers to their peripheries, so that more impurities get trapped near grain boundaries. This process is common for most materials and is ascribable to lower solubility of foreign atoms and ions in a solid phase as compared with a liquid phase. Mobile ions trapped in the ice bulk then diffuse against the gradient of their concentration, generating electrical charge transport and an intrinsic electrical field in ice. In thermal equilibrium, that diffusion flux $j_D$ is canceled with a drift flux of the ions $j_{DR}$

$$j_{DR} + j_D = 0 \qquad (29)$$

where

$$j_{DR} = \frac{e_i}{|e_i|} \mu_i n_i E \qquad (30)$$

$$j_D = -D_i \nabla n_i = -\frac{\mu_i k_B T}{|e_i|} \nabla n_i \qquad (31)$$

where $\mu_i$ = ion mobility
$\quad D_i$ = ion diffusion coefficient
$\quad n_i$ = ion concentration
$\quad e_i$ = ion electric charge.

Equalizing the right-hand sides of eq 30 and 31, we find the intrinsic electrical field

$$E = \frac{k_B T}{e_i} \nabla \ln(n_i). \qquad (32)$$

Such an electrical field oscillates from grain to grain in the ice bulk following grain configurations and is very significant even in non-doped ice grown from distilled water, $E = 100 - 1000$ V/m. In doped ice $E$ can locally be as large as $10^4$ V/m (Petrenko 1992a, 1994b).

When an ice mass is split by a crack rapidly growing in the direction perpendicular to the electrical field, the field generates two surface charges of the opposite sign $\pm\lambda_s$ on the opposite surfaces of the crack

$$\lambda_s = \varepsilon_0 (\varepsilon_s - 1) E_\perp \qquad (33)$$

where $E_\perp$ is a component of the electrical field perpendicular to the crack surface. Inside the crack the same component, $E_\perp^{cr}$, exceeds $E_\perp$ by two orders of magnitude

$$E_\perp^{cr} = \varepsilon_s E_\perp \qquad (34)$$

since $\varepsilon_s \approx 10^2$. Taking $E_\perp = 10^2 - 10^3$ V/m, we obtain a potential difference $\Delta\varphi$ across a 1-mm wide crack

$$\Delta\varphi \approx 10 - 100 \text{ V}. \qquad (35)$$

Such a large potential difference can easily explain why the intrinsic electrical field dominates among the causes of EME from cracks in ice.

The processes of dielectric relaxation causes the density of crack surface charges to decay with time. In the case of a growing crack, this density, thus, decreases as the distance from the crack tip increases. Hence, eq 33–35 are applicable only in a crack tip's vicinity. To calculate $\lambda_s$ far from the tip, we should take into account two processes of relaxation of electrical charges in ice (Jaccard 1964, Gluschenkov and Petrenko 1993, Petrenko 1993a). In the first relaxation process, $\lambda_s$ decays exponentially with time from its initial value $\lambda_s$ to

$$\frac{\varepsilon_\infty}{\varepsilon_s} \lambda_s \approx \frac{1}{30} \lambda_s.$$

The relaxation time of this fast process is

$$\tau_1 \approx \frac{\varepsilon_\infty \varepsilon_0}{\sigma_\infty}. \qquad (36)$$

At $T = -10°C$ in pure ice, $\tau_1 \approx 10^{-6}$ seconds and is even shorter in natural ice. Since the crack velocity in freshwater ice varies in the range from $10^2$ to $10^3$ m/s (Petrenko 1992a, Sato and Wakahama 1992), the length of a high-density surface charge train behind a crack tip is about $10^{-6}$ s $\times(10^2–10^3)$ m/s = 0.1–1 mm.

The rest of the surface charge relaxes very slowly with a relaxation time $\tau_2$

$$\tau_2 \approx \frac{\varepsilon_s \varepsilon_0}{\sigma_s} \tag{37}$$

which is about 0.1 second in pure ice. That means that a crack moving with $10^3$ m/s velocity can have a 100-m long electrically charged tail.

Since the intrinsic electrical field is an oscillating function of the crack length (see Fig. 17), so is the surface charge and the resulting electrical dipole moment of the crack. When a crack grows, its total dipole moment oscillates and generates an EME. An average frequency of EME $f$ relates to the crack velocity $v_{cr}$ and an average grain size $g$ as

$$f = \frac{v_{cr}}{g}. \tag{38}$$

This relationship provides an investigator with a simple method of crack velocity determination using measurements of $f$ and $g$ (Petrenko 1992a, Gluschenk-ov and Petrenko 1993). The dielectric relaxation reduces $\lambda_s$ and should be taken into account. Readers can find more details of the theory of such EME in some previous papers (Petrenko 1992a, Gluschenkov and Petrenko 1993).

*EME from the pseudo-piezoelectric effect*

The second important mechanism resulting in crack-induced electrical polarization of ice is the pseudo-piezoelectric effect discussed above (see eq 20–27 and Fig. 15b). A theoretical description of such polarization was developed earlier (Petrenko 1993a).

When a crack appears and expands, it generates strains in the surrounding material that we define as $\varepsilon_{ij}(\vec{r}, t)$, which depend upon coordinates $\vec{r}$ and time $t$. We have to find the electrical field strength $\vec{E}(\vec{r}, t)$ and electrical potential $\varphi(\vec{r}, t)$ that are caused by these elastic strains. The charge carriers have to move because their energy $U$ depends on strains

$$U = U_0 + U_1(\varepsilon_{ij}). \tag{39}$$

In a linear approximation for an isotropic material

$$U \simeq U_0 - \alpha_{aj} \sum_{i=1}^{3} \varepsilon_{ii} = U_0 - \alpha_{aj} \cdot \varepsilon_{ii}, \quad |\varepsilon_{ii}| << 1 \tag{40}$$

where we use the Einstein summation convention

$$\sum_{i=1}^{3} \varepsilon_{ii} = \varepsilon_{ii}. \tag{41}$$

The constants $\alpha_{aj}$ are usually called the deformation potential constants and for a quite wide variety of materials these constants are about 10 eV.

The force acting on charge carriers in the presence of a strain gradient is

$$\vec{F} = -\text{grad}(U) = \alpha \, \text{grad}(\varepsilon_{ii}) = \alpha \nabla \varepsilon_{ii}. \tag{42}$$

This force initiates a flux of the charge carriers, i.e., electrical currents, and as a consequence an electrical potential difference appears, as in the case of the bending of ice samples (Evtushenko et al. 1984, 1987).

To find the electrical field in the area around a crack, we first find a vector of polarization $\vec{P}(\vec{r}, t)$. Let us consider ice with four types of charge carriers. Then

$$\frac{\partial \vec{P}}{\partial t} = \dot{\vec{P}} = \sum_{j=1}^{4} e_j \vec{j}_j \tag{43}$$

where fluxes $\vec{j}_j$ are determined by the transport equation

$$\vec{j}_j = \left(e_j \vec{E} - \eta_j \Phi \vec{\Omega} + \alpha_{aj} \nabla \varepsilon_{ii}\right) \frac{\sigma_j}{|e_j|^2} - D_j \nabla n_j \tag{44}$$

where $\sigma_j = |e_j| \, \mu_j \, n_j$ are the partial conductivities and $D_j$ are the diffusion coefficients.

Inside the bulk material

$$\text{div} \, \vec{E} = -\text{div} \, \vec{P} / \varepsilon_\infty \varepsilon_0. \tag{45}$$

Taking into account that curl $\vec{E} = 0$ (quasi-stationary approximation) and that at infinity ($r = \infty$) $\vec{E} = \vec{P} = 0$, we can find

$$\nabla \varphi = -\vec{E} = \vec{P} / \varepsilon_0 \varepsilon_\infty. \tag{46}$$

If for a particular crack, the deformation $\varepsilon_{ii}(\vec{r}, t)$ is known, then the system of eq 43–46 is complete. In the presence of dielectric/conductor or conductor/conductor interfaces, we have to join the proper boundary conditions to this system of equations. The system of eq 43–46 has analytical solutions for many cases of practical interest that will be shown in the following sections.

Figure 18 illustrates three types of elementary cracks. Notice that the mode III crack does not produce an electrical field since, for an isotropic material, $\varepsilon_{ii} = 0$ (see for example Hellan 1984).

For a mode I crack

$$\varepsilon_{ii} = K_I \frac{(1-\nu)}{E} \cdot \frac{\cos \frac{\theta}{2}}{\sqrt{2\pi r}} \tag{47}$$

15
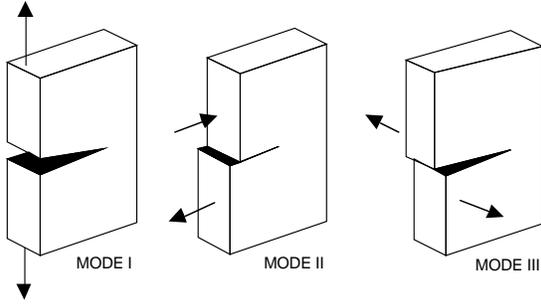
*Figure 18. Three modes of cracks.*

where $\nu$ is Poisson's ratio, $E$ is Young's modulus and $K_I$ is an intensity factor

$$K_I = \beta\sigma(\infty)\sqrt{\pi l} \qquad (48)$$

where $\sigma(\infty)$ is tensile stress at infinity and $l$ is the crack length. The numerical coefficient $\beta$ depends on boundary conditions and is about 1. For the mode II crack

$$\varepsilon_{ii} = K_{II}\frac{(1-\nu)}{E}\cdot\frac{\sin\dfrac{\theta}{2}}{\sqrt{2\pi r}} \qquad (49)$$

$$K_{II} = \beta\tau(\infty)\sqrt{\pi l} \qquad (50)$$

where again $\beta$ is about 1 and $\tau(\infty)$ is shear stress at infinity (Hellan 1984).

For stable cracks or cracks that move "slowly," i.e., cracks for which the time of their motion is longer than the electrical relaxation times, the system of eq 43–46 has a solution (Petrenko 1993a)

$$\vec{E} = \left[\frac{-\nabla\varepsilon_{ii}\cdot\left(\dfrac{\alpha_j\sigma_j}{e_j}+e_jD_j\nabla n_j\right)}{\sigma_j}\right]\bigg/\left(1+\frac{\Phi\varepsilon\varepsilon_o}{e_j^2}\right). \qquad (51)$$

Figure 19 shows force lines of an electrical field generated by mode I and mode II cracks in ice. Estimates made using eq 47–51 show that a typical electrical potential difference between infinity and a crack increases from 10–100 mV at the crack's tail to about 1 V at the crack's tip.

The electrical field generated by a rapidly growing crack can be calculated as

$$\vec{E} = (t,\vec{r}) = -\frac{1}{\varepsilon\varepsilon_0}\exp(-t/\tau_1) \qquad (52)$$

$$\int_0^t\left[\exp(\xi/\tau_1)\right]\frac{\alpha_j\sigma_j}{e_j}\nabla\varepsilon_{ij}(\xi,\vec{r})d\xi$$

where $\tau_1$ is the fast relaxation time from eq 36 and the $j$th type of charge carriers are majority charge carriers.

**Laboratory experiments**

Today, we have an ample collection of experimental data on the generation of EME and electrical signals by cracks in ice. To the best of our knowledge, the first laboratory[0] measurements of electrical signals from cracks were performed by Takahashi (1969b). He measured an electrical charge generated by the breaking of frost under a temperature gradient. The frost was grown either between two ice hemispheres or between two metal plates. Significant charge separation was observed only under a temperature gradient, which generates an electrical field $E_\perp$ in the direction perpendicular to the cracks in the frost. The strength of electrical field $E_\perp$ of about 20 V/m at –15°C was generated by the thermoelectric effect in ice. The density of the electrical charge separated by cracks in frost was estimated by Takahashi as $10^{-6}$ C/m. That value exceeds by about one order of magnitude the charge density predicted by eq 33. The discrepancy may be explained by the break in the frost occurring at the narrowest neck, where the temperature gradient, and hence $E_\perp\propto\nabla T$, exceed their average magnitudes.

Takahashi (1983) expanded his study of charge separation by cracks in single-crystalline ice samples. During those experiments, both sample cross section and the temperature gradient were well defined. Again,
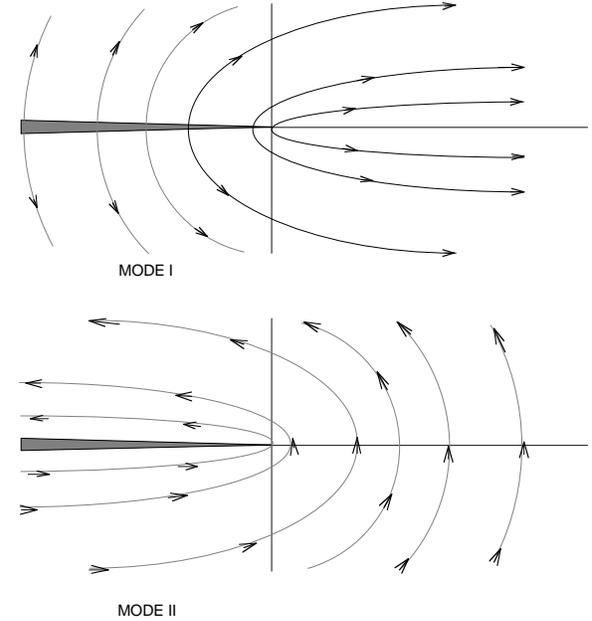


*Figure 19. Lines of force of the electric field induced by stable mode I and mode II cracks in ice (after Petrenko 1993a).*

16

though there was large scattering in the data, significant charge separation was observed only in the presence of a temperature gradient $\nabla T$ and, hence, $E_\perp$. An average of that set of the results fits well to the prediction given by eq 33.

Electrical signals from thermocracks in ice single- and polycrystals were studied by del Pennino et al. (1974). Their ice specimens were frozen on the top of a massive copper substrate that was also used as the first electrode. The second electrode, connected to a lock-in amplifier, was vibrated above the ice surface to measure the ice–metal contact potential (Kelvin method). Thermocracks were produced during intensive cooling of the copper substrate because of the difference in the thermal expansion coefficients of copper and ice. The cracks in the ice (which were assumed to be mode I type) grew in prismatic planes of ice single crystals, starting from the copper substrate toward the mobile electrode. Figure 20 depicts several such events. The potential jumps associated with crack nucleation measured from one to several volts and were characterized by very long relaxation time. The relaxation time varied from $10^2$ seconds at $-20°C$ to $10^4$ seconds at $-100°C$. While the signals' amplitude can be explained in terms of the pseudo-piezoelectric polarization of ice induced by cracks, their too-long relaxation time does not correspond to any electrical relaxation time known for ice. That time may correspond, as the authors suggested, to relaxation of elastic stress in ice.

Fifolt (1990, 1991) and Fifolt et al. (1992, 1993) found and investigated electrical signals from cracks in freshwater columnar and granular ice under uniaxial compression. Temperature gradients and other possible sources of external electrical fields were absent in these well-controlled experiments. The measurements were performed in a temperature range from $-10$ to $-33°C$. Electrical signals from cracks appeared as an
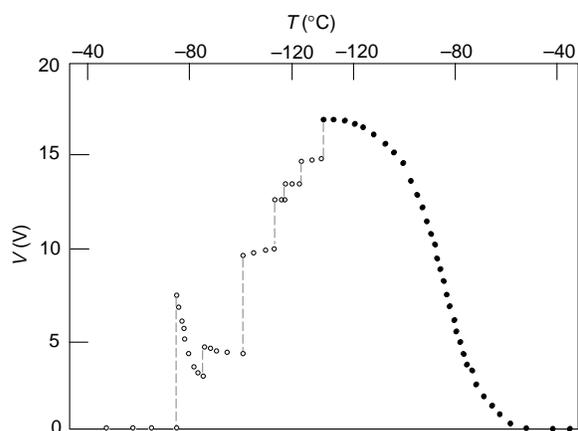


Figure 20. Jumps of electric potential V caused by nucleation of thermocracks (after del Pennino et al. 1974). Open circles show V during freezing at a constant rate of 0.5°C/min; solid circles show V under warming at a rate of 0.35°C/min.

electrical potential difference between two metal electrodes, which were either attached to an ice specimen (thin foil electrodes) or placed at some distance from the specimen surfaces (see Fig. 21).

Observed signals ranged in amplitude from 4 to 70 mV and lasted from $1.5 \times 10^{-4}$ to $10^{-2}$ seconds. Most commonly, the signals exhibited an exponentially decaying form (Fig. 22). Independent measurement showed that the signals' delay time coincided with the slow dielectric relaxation time $\tau_2$ (see eq 37). The signal type shown in Figure 22 was typical for small cracks that either split one ice grain or were located on one intergranular boundary. Oscillating, sinusoidal type signals were characteristic for large cracks that split many single-crystalline grains or columns (Fig. 23).

The nature of such signals was understood after the discovery of the frozen-in, intrinsic electrical field in polycrystalline ice (Petrenko 1992a). Cracks in such ice



a. Ice sample and electrodes.
b. Synthane endcaps.
c. RF shielded enclosure.
d. High input impedance preamplifier.
e. Digital storage oscilloscope.
f. Computer.
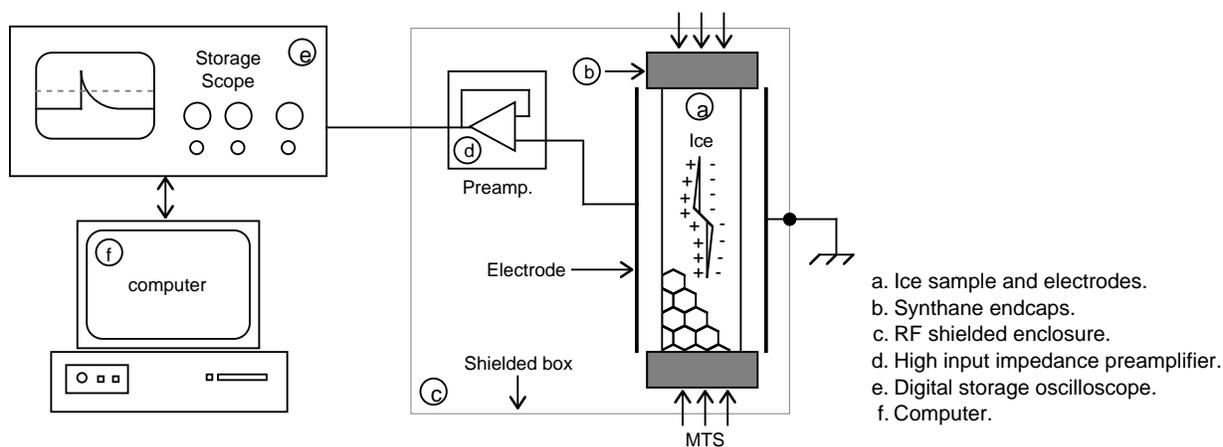
Figure 21. Signal recovery system used to detect emissions (after Fifolt et al. 1993).
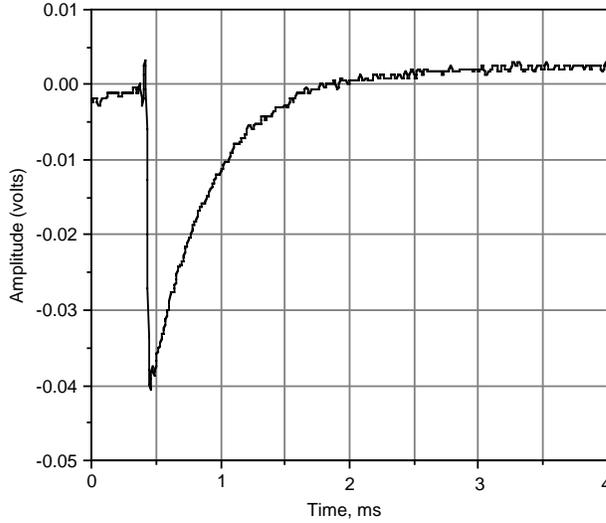
Figure 22. Electrical signal of a microcrack in freshwater columnar ice (after Fifolt et al. 1993). T = –33°C, σ = 6.3 MPa.
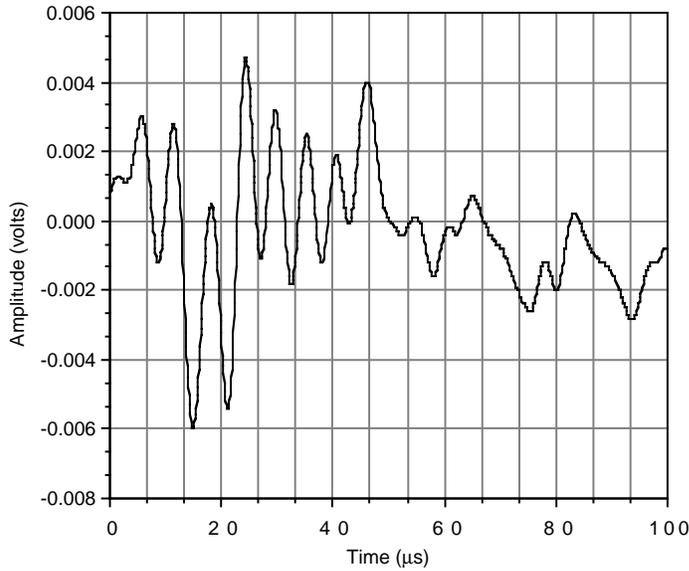


Figure 23. Electrical signal of a large crack splitting many columns in freshwater columnar ice (after Fifolt et al. 1993). T = –30°C, σ = 3.78 MPa.

split electrically pre-polarized ice, causing the appearance of growing or oscillating electrical dipoles (see the theoretical section above). This mechanism was later proven in experiments in which a strong external electrical field was applied to ice samples with growing cracks (Petrenko 1993d). It was shown that in this case the magnitude of electrical signals from cracks is proportional to the external electrical field $E_\perp$, in accordance with eq 33. An example of a signal generated by a microcrack in the presence of an external electrical field is shown in Figure 24. Again, the decay time of the signals coincided with the slow dielectric relaxation time $\tau_2$.

Electrical polarization of ice, induced by a stable crack, attributable to the pseudo-piezoelectric effect, was studied using the scheme depicted in Figure 25 to determine electrical field distribution around the crack (Petrenko 1992a). Narrow cracks prepared by a thin
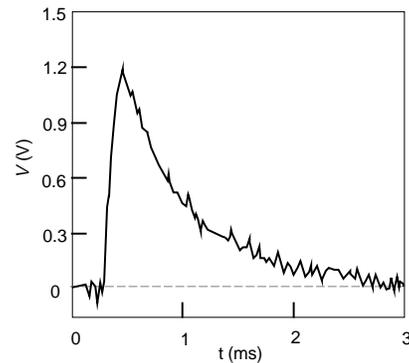


Figure 24. Typical electrical signal captured from a microcrack in freshwater ice under the action of an external electric field $E_\perp = 10$ V/cm. T = –10°C, crack dimensions $2 \times 2$ cm (after Petrenko 1992a).

18
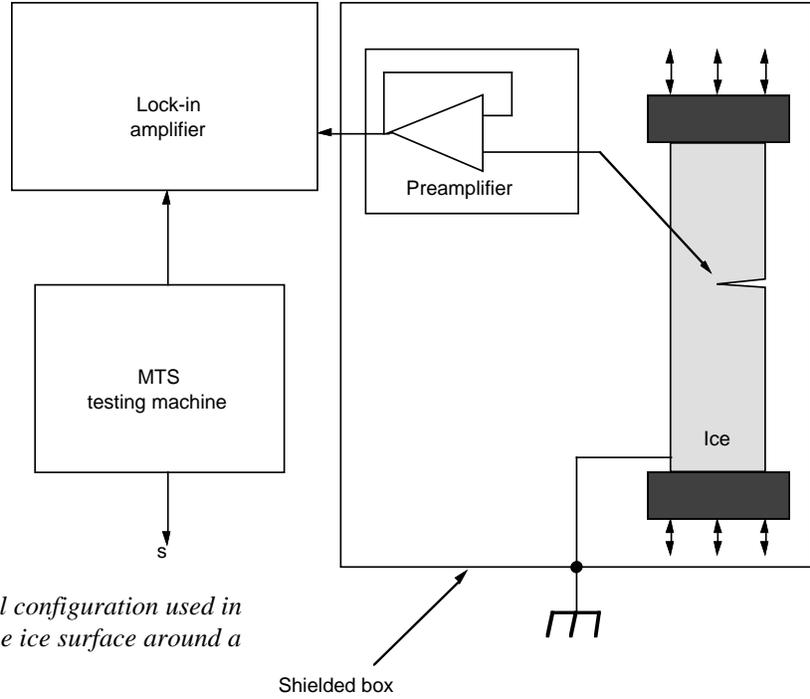
*Figure 25. Schematic of experimental configuration used in measurements of electric fields on the ice surface around a stable crack (after Petrenko 1992a).*

bandsaw (1 mm thick) were located in the middle of the samples, perpendicular to their long side. Sample dimensions were $15 \times 6 \times 6$ cm$^3$ and the crack length varied from 5 to 30 mm. An oscillating sine wave, of frequency from 1 to 300 Hz, was applied to the samples by an MTS testing machine. In this set of measurements, a sine potential difference was measured by a lock-in amplifier between one remote electrode mounted into the ice and one electrode placed near the crack tip. This latter electrode in some cases was mounted into the ice to a depth of 2 mm, by careful heating of the electrode, or was attached to the ice surface with slight pressure. The electrodes were made of stainless steel wire of 0.1-mm diameter.

Figure 26 shows the distribution of the amplitude of an oscillating electrical potential $\varphi$ measured around an artificial mode I tearing crack. To compare these experimental results with the theory, $\varphi$ was calculated using eq 51

$$\varphi = \frac{\varepsilon_{ii} \alpha_j}{e_j + \dfrac{\Phi \varepsilon \varepsilon_0}{e_j}} \qquad (53)$$

where $\varepsilon_{ii}$ must be taken from eq 47 and $\alpha_j = \alpha_4 = 6.2$ eV (Evtushenko et al. 1987). There is satisfactory quantitative and qualitative agreement between theory and experiment in the vicinity of the crack tip for $r = 1$–10 mm. At $r = 1$ mm, $\varphi = 0.8$ mV. Yet, at larger distances $\varphi$ remains almost constant instead of decreasing to 0 as the theory predicts ($\varphi \propto r^{-1/2}$; $r$ is the distance
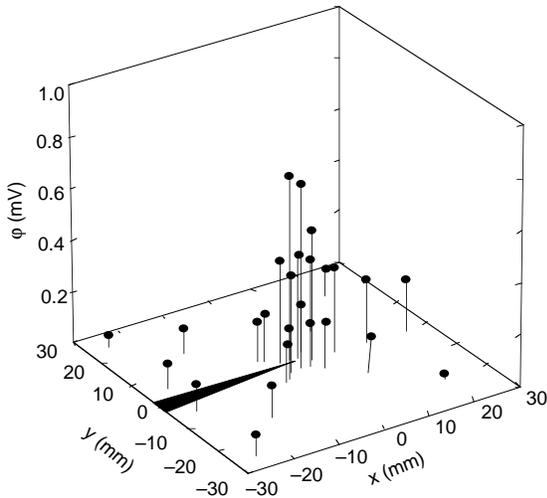


Sample dimensions $13 \times 6.5 \times 6.5$ cm
Crack length $l = 3$ cm
Width $d = 1$ mm
$T = -10°$C
Stress amplitude 0.12 MPa
Frequency 90 Hz

*Figure 26. Amplitude of electric potential $\varphi$ on the surface of the ice sample measured in the configuration shown in Figure 25; large grains of ice grown from deionized water (after Petrenko 1992a).*

19

to the tip). This discrepancy could arise from small oscillations of the crack surfaces if there is a constant potential difference between them.

Similar EME from cracks were observed by Thiel (1992). He recorded EME in the vicinity of ice cracks created by breaking rods of ice, scouring the ice surface, applying uniaxial pressure to a cylindrical ice core and using a bore-hole jack in an ice sheet. The observations were made in the frequency band from 50 Hz to 15 kHz, using a two-channel audio cassette recorder and wire probes inside or outside the ice. Thiel found that EME events correlate with acoustic emissions events that arise during crack formation.

### Field experiments

At present we have several reports on observations of EME from lake ice, glaciers and sea ice sheets. Kachurin et al. (1979) reported the detection of electrical and magnetic signals from ice and snow under field conditions. Radio waves emitted by the motion of snow avalanches were recorded by a set of radio-frequency receivers working in the frequency ranges of 0.1 to 30 Hz, 900 Hz to 2 kHz, 2.5 MHz, 40 MHz and 760 MHz. The electrical component of EME was recorded at 760 MHz, and the magnetic component at the other frequencies. The sensitivity of the detectors over all frequencies was 1 to 2 μV/m. Broadband EME with a maximum near 1 kHz were recorded for avalanches of freshly fallen snow and near 2.5 MHz for packed snow. The amplitudes of the electromagnetic signals investigated were one to two orders of magnitude higher than that of background noise in the same corresponding range. The authors did not provide information either on the distance from the receiver to the avalanches nor on the types of antenna used. While all the mechanisms of EME from ice considered above are applicable for numerous cracks in a snow cover during an avalanche, there may be some additional phenomena, such as frictional electrification, responsible for the EME from snow avalanches.

The same authors reported detection of magnetic signals captured from a mountain glacier (Malyy Azau glacier in the Caucasus Mountains) during various natural and artificially induced dynamic processes. The EME and seismic signals were recorded in the 0.1- to 30-Hz frequency range. The magnetic component was captured with a single-turn loop with a diameter of 100 m and with an induction coil with a Permalloy core. Figure 27, taken from the paper by Kachurin et al. (1979), shows the correlation between EME and seismic signals captured from the glacier. Later, Kachurin et al. (1984) reported EME from freshwater lake ice and sea ice sheets. To measure the horizontal component of the magnetic field, they used an induction coil with a resonance frequency of 10 Hz. The EME from lake ice were detected during air cooling at night and during ice hummocking. In the same study Kachurin and his co-authors measured quasi-static ($10^{-2}$ to 1 Hz) electrical fields generated in first-year sea ice during its loading. When the load was applied they detected an electrical potential difference of a few millivolts between two electrodes mounted into the ice at a distance of 50 m from each other. The corresponding bend of the ice sheet was about $10^{-4}$ radian.

They also made a very interesting attempt to detect sea ice EME from an airplane flying at an altitude of 100
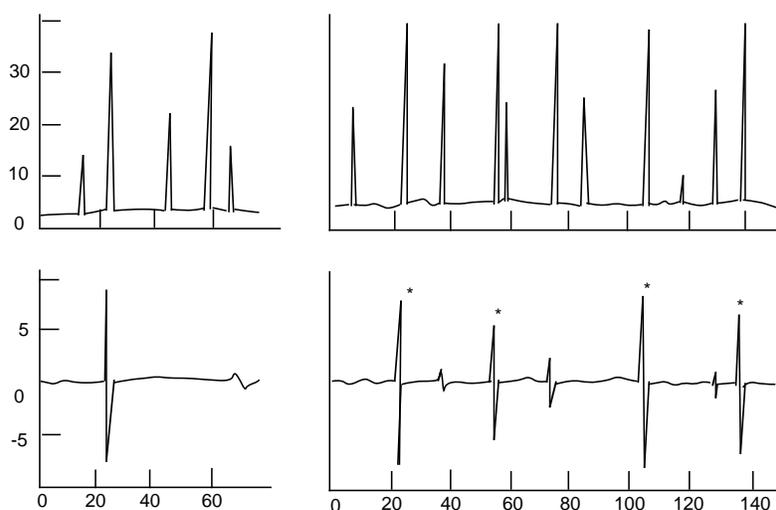


*Figure 27. Synchronous records of the electromagnetic (top) and seismic (bottom) signals captured from natural and artificially induced glacier tremors on 17 August 1977 (after Kachurin et al. 1979). The pass band of the electromagnetic and seismic signals is 0.1 to 30 Hz.*

Figure 28. Synchronous 3-day en route measurements of electric (top) and magnetic (bottom) fields (after Kachurin et al. 1988).

1. Fast 1-year ice, 100–130 cm, snow 20 cm, hummocks
2. Marine ice 60–80 cm, hummocks, snow 20 cm, compression
3. Ice fields with open pools
4. Fresh, snow-free ice 30–40 cm, compression
5. Large open pools, ice-free water, tow vessel released and 180° turn made
6. Fresh ice with open pools
7. Ice fields with open pools
8. Passage into solid ice.

m using a magnetic ferrite antenna connected to a selective amplifier. The amplifier was tuned to the frequency of 100 kHz. An equivalent sensitivity of the measuring system equaled 2 $\mu$V/(mV/m), and an equivalent noise level was 0.3 mV/m. The plane flew above various regions such as open water, thin ice and thick ice during different wind conditions. Strong wind loads the ice, causing intensive cracking, hummocking and deformation. They found that the strength of the electromagnetic field increased to 5–8 mV/m above the regions with intensive ice deformation, while without wind loading or above open water, variations of EME did not exceed 0.5 mV/m as measured on different days.

During the navigation period of 1986, the electrical and electromagnetic fields arising from a fracturing of the ice cover during ship passage were measured from the nuclear icebreaker *Arktika* (Kachurin et al. 1988). A dynamic electrometer was used for the measurements of electrostatic fields in the range of 10 to $10^5$ V/m. The electrometer was on a movable arm mounted 11 m above the waterline at the bow of the icebreaker. Electromagnetic pulses were recorded with an induction transducer having a ferrite core with a resonance frequency of about 1 kHz. The signals were amplified by a selective microvoltmeter in the frequency range from

200 Hz to 2 kHz. The researchers picked this frequency range to minimize the level of natural and industrial electromagnetic interference and to allow subsequent satellite measurements through the ionospheric radio propagation window in the ELF range. An equivalent ambient noise was about $10^{-10}$ T while the signals usually measured from ice fracture exceeded $10^{-9}$ T.

Figure 28 shows the results of synchronous measurements of the electrical and electromagnetic fields made in ice sheets of various thicknesses and ages. Icebreaker velocity and electrical and magnetic field strengths correlated over a much shorter time scale of several minutes. The electrical and magnetic fields measured in these experiments may be caused by both EME from cracks and frictional electrification of ice and snow generated by the icebreaker passing through the snow-covered ice.

Petrenko and Gluschenkov (1995) reported field measurements of EME from individual cracks in freshwater lake ice, and Gluschenkov and Petrenko (1993) did the same with first-year sea ice. The electrical component of the EME from cracks was measured with an experimental setup shown schematically in Figure 29. A 10-m-long dipole antenna was stretched horizontally 1 m above the ice surface. The antenna was connected to an input circuit with a high input impedance ($10^{14}$ $\Omega$) preamplifier. The high input impedance together with the electrical capacitance of the antenna (~$10^{-11}$ F) enabled us to measure electrical fields in a wide frequency
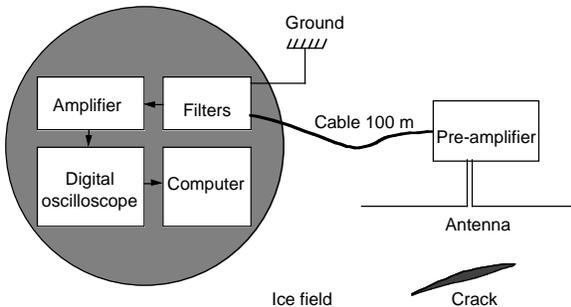


Figure 29. Experimental configuration used in measurements of EME from cracks in lake and sea ice (after Gluschenkov and Petrenko 1993).

21
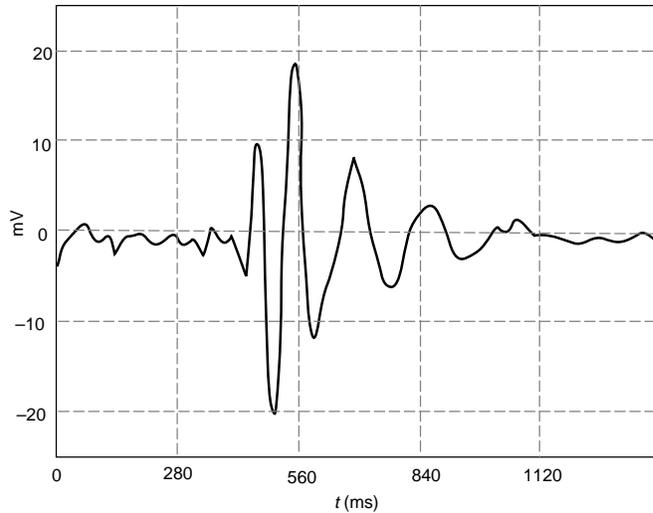
Figure 30. Typical signal captured from a thermo-crack grown in lake ice (after Gluschenkov and Petrenko 1993). T = –5°C.
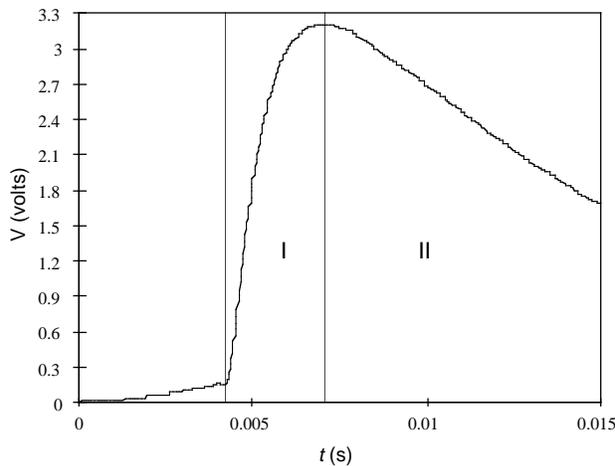


Figure 31. Electromagnetic emission from a crack in sea ice (after Petrenko and Gluschenkov 1995). The crack was 60 cm long and 10 cm wide. Area I corresponds to the crack propagation and area II corresponds to electrical relaxation of the electric field after crack arrest.

range, from about $10^{-3}$ Hz to 1 MHz. Additional filtering was used to cut off the common industrial (60 Hz) and ionospheric ($f \geq 100$ kHz) noise.

Most of the signals captured from identified cracks were very similar to those found in the laboratory (Petrenko 1992a, Fifolt et al. 1993). A typical signal captured from a thermocrack in freshwater columnar lake ice is depicted in Figure 30. The crack appeared 10 m from the antenna and split several single-crystalline columns of ice. As in the laboratory experiments, the oscillation of the electrical field can be interpreted in terms of an oscillating electrical charge on the crack surfaces.

An electrical signal captured by a dipole antenna from a larger crack splitting a cold (–35°C) plate of sea ice is shown in Figure 31. The crack surface was normal to the direction of the gradient of salinity of the ice, and hence the crack grew perpendicular to the frozen-in intrinsic electrical field. Again, as in corresponding laboratory experiments, the signal increases during crack propagation and then relaxes after crack arrest.

## ELECTROPLASTIC EFFECTS IN ICE

Several electromechanical phenomena in ice are associated with the motion of electrically charged dislocations. They are all of quite small magnitude. Nevertheless, their significance is determined by their contribution to the study of the physical mechanisms that govern motion of dislocations and, hence, plastic deformation of ice. Electrically charged dislocations were found in many materials such as ionic crystals (see review by Whitworth 1975); covalent semiconductors (see review by Alexander and Teichler 1991); and crystals with mixed covalent–ionic bonding (see review by Osip'yan et al. 1986). In these materials the electrical charge on a dislocation core appears when a dislocation captures either charged point defects (such as vacancies and interstices in ionic crystals) or electrons (or holes), as happens in semiconductors or when both point defects and electrons (holes) are captured. Significant theoretical efforts have been applied to clarify the formation of the dislocation charges in ionic
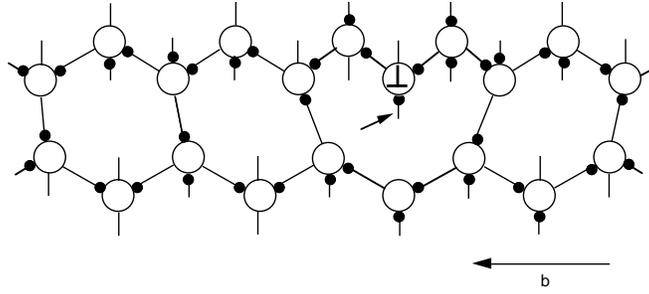
*Figure 32. Section in the $(1\bar{1}00)$ plane of a 60° dislocation on a plane of the shuffle set in the structure of ice, illustrating the dangling bond in the core.*

materials and semiconductors. Though there are no theoretical papers on the electrical charge of dislocations in ice, some reasons for formation of such a charge are obvious.

First, the charge may originate from electrical activity of dangling hydrogen bonds in the dislocation core. Figure 32 illustrates a dangling bond in the core of a 60° dislocation. A dangling bond may or may not have a proton on it. In the first approximation, the probability of finding a proton on a dangling bond is 50%, since when a regular hydrogen bond breaks into two dangling bonds, one proton is shared between two bonds. It is generally acknowledged that a regular hydrogen bond is electrically neutral. The dangling bonds of a dislocation core introduce electron energy levels or narrow energy bonds located in the forbidden band of ice. Depending on the relative position of a Fermi level and the dislocation levels (bands), the exchange of electrons between the dangling bonds and the bulk ice will result in a net negative or positive charge of the dislocation. It is not known at present if such dangling bonds may exchange protons with an ice bulk.

Second, a mechanism that may result in a net dislocation charge is strong elastic interaction between a protonic charge carrier—i.e., ions and Bjerrum defects—and strain generated by a dislocation. Figure 33 illustrates stress patterns in the vicinity of an edge dislocation. As is seen from this figure, the dislocation generates compression in the upper quadrants and tension in the lower ones.

The specific volumes of protonic charge carriers (ions and Bjerrum defects) exceed that of a water molecule (Evtuschenko et al. 1987, Evtuschenko and Petrenko 1991). Thus, all these charged defects should accumulate in the lower quadrant and escape from the upper one. Figure 34 shows schematically the change in defect activation energy as a function of the $x$ coordinate, also shown in Figure 33. Since for the protonic defects in ice $\alpha_i$ ranges from 1.2 to 6.8 eV and $\varepsilon_{ii}$ is about 0.1 in the vicinity of a dislocation core, the binding energy, $\alpha_i \varepsilon_{ii}$, of the defects on an edge dislocation
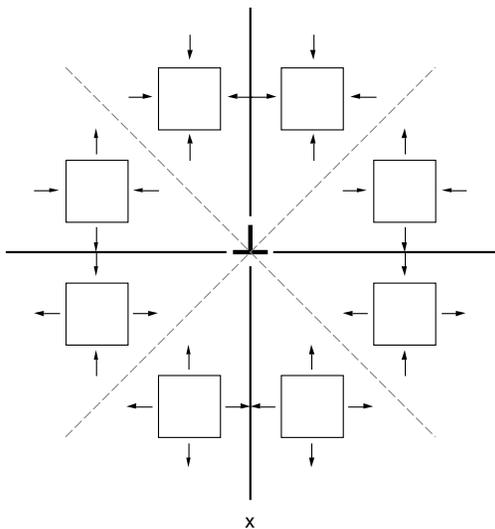


*Figure 33. Directions of the principal stresses in the vicinity of an edge dislocation. The dislocation line is directed perpendicularly to the figure's plane.*
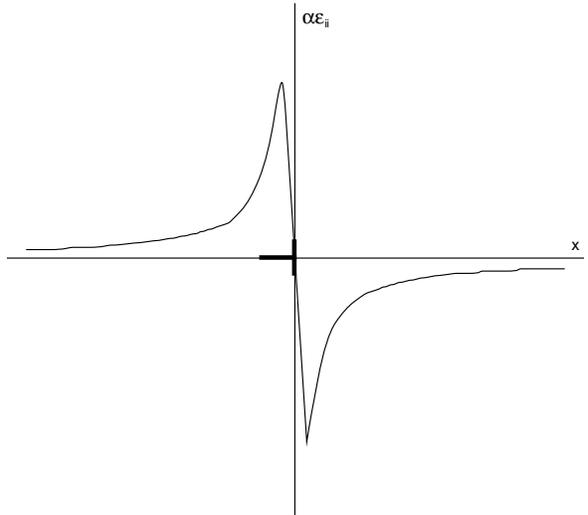


*Figure 34. Change in activation energy $\alpha\varepsilon_{ii}$ of a charge carrier in ice in the vicinity of an edge dislocation.*

23

is about tens of electronvolts and is comparable with the defects' activation energy. That should result in significant buildup of defects near a dislocation and in total electrical charge if $\alpha_i$ differs for positive and negative defects. Such a mechanism of dislocation charge creation was first suggested and estimated in Petrenko and Ryzhkin (1986a,b), but has never been accurately calculated.

Electrically charged dislocations can manifest themselves in three different electromechanical phenomena. First, their motion during plastic deformation can result in an electrical current, a so-called dislocation current. Second, application of an external electrical field may cause the dislocation motion and, hence, small plastic deformation. Third, the introduction of dislocations may change concentrations of charge carriers and, as a result, cause a change in electrical conductivity and dielectric permittivity of ice. We will consider below all three groups of phenomena.

**Dislocation currents in ice**

Dislocation currents in ice were measured and used for determination of the linear density of dislocation charge $q$ (Petrenko and Whitworth 1983). We used specimens of very pure single crystals of ice in which the majority of edge dislocations of one mechanical sign was introduced by preliminary bending, as shown in Figure 35a. A smaller ice sample was then cut off the bent specimen for tensile tests (Fig. 35b and c). The electrodes were formed from an Hg-In amalgam, which adheres well to the surface of ice but remains liquid down to –30°C, so that it does not interfere with deformation. Dislocation currents were measured with an electrometer at $T = -20°C$ during tensile creep of the ice samples. A typical recording of both the current $I$ and the tensile elongation $\Delta\ell$ are shown in Figure 35d. The abrupt changes in the current $\Delta I$ were caused by the starts and stops of charged dislocations. It was shown that $q$ can be calculated as

$$q = \frac{\Delta I b_z}{\dot{\ell}_p d} \tag{54}$$

where $b_z$ = component of the Burgers' vector along the length of the specimen
   $d$ = interelectrode distance
   $\Delta I$ = dislocation current
   $\dot{\ell}_p$ = rate of the tensile plastic deformation.

The dislocation charge may be expressed in terms of $qa/e$, i.e., in the number of elementary charges per intermolecular distance $a$. We found that the dislocation charge in ice was positive, with an absolute magnitude of $qa/e = 2 \times 10^{-3}$. That corresponded to two proton



a. Bent crystal containing an excess of dislocations of one sign. When deformed by tension the majority of dislocations move toward the upper electrode $E_1$.

b. How the tensile specimen is cut from the bent crystal.

c. Ice specimen mounted for tensile deformation experiment.

d. Recordings of change of length $\Delta\ell$ and current I during tensile deformation. Load is applied and removed at times indicated by the arrows. $\Delta\ell$ was measured in micrometers.

Figure 35. Dislocation currents in ice (after Petrenko and Whitworth 1983).

charges per thousand intermolecular distances along the dislocation core. This charge magnitude was estimated as a lower limit because of the use of blocking (non-ohmic) electrodes, so that the charge flow within the ice produced polarization at the surface and the full current may not be recorded by the electrometer.

## Motion of charged dislocations in an electrical field

Itagaki (1970) used a different technique to determine the dislocation charge density $q$. Using X-ray topography to observe dislocation lines in ice, he found that some dislocations vibrated when an external ac electrical field was applied. At the low-frequency limit, the amplitude of vibrations $\eta$ depends only on the length of a dislocation segment $\ell_d$, external electrical field $E$ and the tension of a dislocation line $T_d$. Namely

$$\eta = \frac{\ell^2 \cdot E \cdot q}{8T_d}.$$ (55)

This equation enables us to estimate $q$ if $\ell$, $\eta$ and $E$ are known.

Itagaki measured the amplitudes of vibrations $\eta$ in pure single crystals of ice taken from the Mendenhall glacier. The ac field strength ranged from 3 to 600 V/cm, and three frequencies of 60, 1.33 and 0.33 Hz were used. The linear density of a dislocation charge estimated by Itagaki ranged from $qa/e = 3.6 \times 10^{-3}$ to $qa/e = 2 \times 10^{-2}$.

Later, Joncich et al. (1978) tried to explore a similar idea to estimate $q$ for dislocations. They applied a strong electrical field across a low-angle title boundary consisting of edge dislocations. Their tests were performed at $T = -15°C$. No measurable displacement of the boundary was observed. Based on their experimental precision, Joncich et al. concluded that $qa/e$ cannot exceed $3.3 \times 10^{-3}$. Since they used a dc electrical field and blocking electrode, the real $E$ in the ice bulk in their experiment could be lower than they ex-

pected. This should increase the estimated upper limit of $qa/e$ somewhat.

We can conclude that there is no significant discrepancy among different authors and the techniques applied and that most probably the magnitude of $qa/e$ should be somewhere in the range from $2 \times 10^{-3}$ to $2 \times 10^{-2}$. If the above-described accumulation of point defects in the region of tension near a dislocation core is responsible for the dislocation charge, then the small linear density of this charge does not reflect the real number of the defects captured, but rather shows a difference in concentrations of positive and negative defects near the dislocation.

## Effect of static electrical field on ice creep

In ionic crystals and some semiconductors, $qa/e$ is so large (0.1–1.0) that the application of high external electrical fields of $E \approx 10^4$ V/cm is able to accelerate or halt creep, depending on the relative directions of $q\vec{E}$ and the predominant velocity of dislocations (Whitworth 1975, Osip'yan et al. 1986). Such an effect of electrical fields on plastic deformation in ice has not been observed so far. However, the application of even smaller static electrical fields of $10^3$ V/cm can significantly suppress plastic creep of thin ice specimens having a thickness of 1 mm or less (Petrenko and Schulson 1993).

We examined the effect of dc and ac electrical fields on the plastic deformation of pure and doped (with HF and KOH) single crystals of ice in the temperature range of –10 to –45°C. The basal plane (0001) was a slip plane for dislocations. We found that a relatively small (about 10–50 V) dc voltage applied across thin single crystals decreased both the creep strain rate $\dot\varepsilon$ and the high-frequency conductivity of ice $\sigma_\infty$. Figure 36 depicts the dependence of the creep strain rate on the dc voltage applied to a 50-$\mu$m thick ice specimen. At the same time, the application of an ac electrical field of the same strength as the dc field or the application of a dc field to thick specimens (1–3 mm) did not reveal changes in the creep rate. We felt that the observed changes in the plastic deformation were ascribable to a decrease in the concentrations of Bjerrum defects caused by the strong static electrical fields. The concentration of Bjerrum defects is proportional to $\sigma_\infty$ and can be easily monitored.
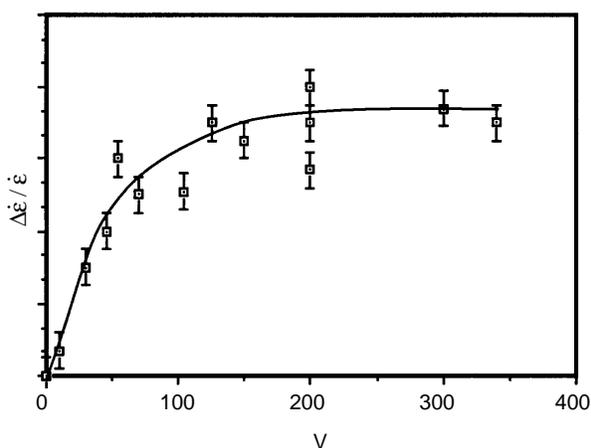
*Figure 36. Dependence of the relative change in strain rate $\dot\varepsilon$ on the applied dc voltage V (after Petrenko and Schulson 1993). $\dot\varepsilon$ is the strain rate at V = 0. T = –20°C, sample thickness L = 50 μm.*

25

**Effect of plastic deformation on electrical properties of ice**

Dislocations introduced during the process of plastic deformation can affect the electrical properties of ice (as well as other materials) in a variety of ways. They can generate new point defects such as vacancies, interstitials and Bjerrum defects; they can also capture point defects by their elastic field and make defects immobile. All this can change the charge carrier concentrations. But this is not the whole story yet. Owing to their long-range elastic and electrical fields, dislocations can effectively scatter charge carriers. As a result the charge carrier mobility usually decreases after plastic deformation. Moreover, charged dislocations may, in principle, move under the action of these electrical fields, contributing to both electrical conductivity and dielectric permittivity.

The first known, but unsuccessful, attempt to find the effect of plastic deformation on the electrical properties of ice was made by Brill and Camp (1957). They reported no changes induced by plastic deformation in the dielectric properties of ice at 1 kHz. On the contrary, Higashi (1969) reported preliminary results obtained by Mae, who found a very profound increase in low-frequency conductivity and dielectric permittivity

of ice that had undergone 15 and 30% plastic deformation (Fig. 37). These changes were confirmed later by Mae and Higashi (1973), after they conducted very detailed and careful investigations on the effect of plastic deformation on ice electrical conductivity and dielectric permittivity in wide temperature ($-10$ to $-100°C$) and frequency (0.5 to $10^3$ Hz) ranges. During plastic deformation of pure single crystals of ice, the dislocation density in their experiments rose from $10^4$ to $10^7$ cm$^{-2}$. Mae and Higashi found that plastic deformation left unchanged the high-frequency conductivity $\sigma_\infty$ but induced significant changes in low-frequency conductivity $\sigma_s$. This can be easily explained, as the plastic deformation generated a concentration of new charge carriers that was comparable with the minority charge carrier concentration but was much less than the majority charge carrier concentration. That would also explain the failure of Brill and Camp, who measured $\varepsilon$ in the region of majority charge carrier frequency.

A typical change in $\sigma_s$ found by Mae and Higashi, after introducing a dislocation density of $10^7$/cm$^2$, was $2 \times 10^{-10}/\Omega \cdot$ cm. Notice that this number, when recalculated into the number of elementary charges per intermolecular length on a dislocation, gives $5 \times 10^{-3}$, which is in the range of the experimental magnitude of *qa/e*.
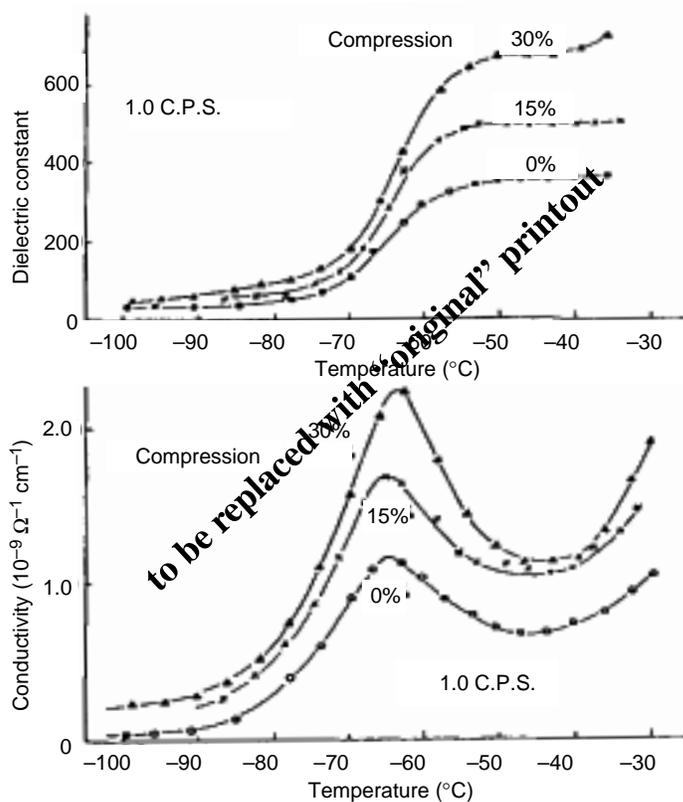


*Figure 37. Effect of compressive strain on the electric properties of ice single crystals, measured at 1 Hz (after Higashi 1969).*

Mae and Higashi also analyzed separately changes in the mobility and concentration of minority charge carriers caused by plastic deformation. They used for this purpose their experimentally obtained frequency dependencies of $\sigma$ and $\varepsilon$, but exploited a theory by MacDonald (1953), which is not applicable to ice. Their results showed unrealistic magnitudes for an ion mobility of 0.6 $cm^2$/V s. Nevertheless, when the same experimental technique is combined with a specific theory for ice (Petrenko and Ryzhkin 1984a), it gives a correct value for mobility of ions, of a few $10^{-3}$ $cm^2$/V s (Zaretskii 1991).

Noll (1978) studied the influence of plastic deformation on electrical properties during and after deformation. He measured $\sigma$ and $\varepsilon$ at $T = -3$ and $-10°C$ in a frequency range from $10^{-2}$ to $10^5$ Hz, a strain rate range from $2 \times 10^{-5}$ to $10^{-3}$ $s^{-1}$, and a strain range from 0.03 to 0.6. He found that plastic deformation reduces the electrical conductivity in the space-charge dispersion frequency range (Fig. 38). The decrease depended strongly on the strain rate, while the strain magnitude
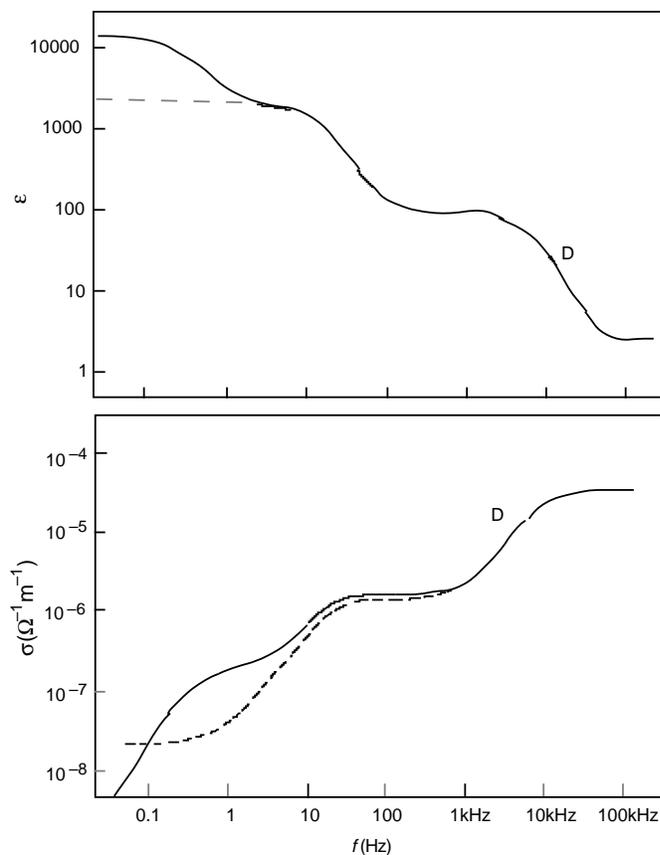
had little effect. After deformation takes place, recovery processes have been observed that restore the original conductivity if the total strain was small. Rapid and large deformation, however, causes permanent changes in the conductivity and dielectric permittivity.

Itagaki (1978, 1982, 1983) conducted a very interesting series of experiments and theoretical calculations aimed at determining the contribution of electrically charged dislocations to the electrical properties of ice. In 1978 he carried out an exciting experiment in which he compared the electrical properties of dislocation-free areas of ice pure microcrystals with areas having a high density of dislocations. He used hoarfrost crystals as the specimens and X-ray topography to visualize dislocations in them. Use of tiny liquid-mercury electrodes prevented damage to the ice crystals. Itagaki did not observe the Debye dispersion of $\sigma$ and $\varepsilon$ in dislocation-free regions, while it was present in the regions with high dislocation density and in the initially dislocation-free regions after introduction of dislocations by surface scratching. On the basis of these observations, he concluded that the main reasons known for the polarization process in ice, the Debye dispersion and hence the high-frequency conductivity $\sigma_\infty$, are related to the motion of charged dislocations in an ac electrical field.

He later developed a theoretical model supporting this idea (Itagaki 1982, 1983). However, Itagaki's model was not accepted by the ice physics community. While dislocations in ice can contribute to and modify the electrical properties of ice, they cannot account completely for those electrical properties. There may be other reasons for the absence of Debye dispersion found by Itagaki in very thin and pure specimens of ice. One possibility is that the specimen thickness was comparable with or less than a screening length. Conventional theories of electrical properties of ice (Jaccard 1964) predict an absence of the Debye dispersion in this case (Petrenko and Ryzhkin 1984a).



Figure 38. Effect of plastic deformation on dielectric permittivity $\varepsilon$ and conductivity $\sigma$ (after Noll 1978). Solid lines were obtained before deformation, dashed lines were obtained during plastic deformation at $\dot{\varepsilon}_p = 3.2 \times 10^{-5}$ s and $\varepsilon_p = 0.274$. $T = 270.2$ K.

## LITERATURE CITED

**Alexander, H. and H. Teichler** (1991) Dislocations. *Materials Science and Technology*, **4**: 249–301.

**Barer, S.S., V.I. Kvlividze, A.B. Kurzaev, V.D. Sobolev and N.V. Churaev** (1977) Thickness and viscosity of thin unfrozen layers between ice and quartz surfaces. *Doklady Akademii Nauk USSR,* **235**(3): 601–603.

**Barnes, P., D. Tabor and J.C.F. Walker** (1971) The friction and creep of polycrystalline ice. *Proceedings, Royal Society,* **A325**: 127–155.

**Brill, R. and P. Camp** (1957) Influence of pressure on the dielectric properties of ice. *Nature,* **179**: 623–462.

**Brook, M.** (1958) Laboratory study of charge separation during ice–ice contact. In *Recent Advances in Atmospheric Electricity* (L.G. Smith, Ed.). London: Pergamon Press.

**Bryant, G.W. and N.H. Fletcher** (1965) Thermoelectric power of ice containing HF or $NH_3$. *Philosophical Magazine*, **12:** 165–176.

**Buser, O. and C. Jaccard** (1978) Charge separation by collision of ice particles on metals: Electronic surface states. *Journal of Glaciology,* **21**(85): 547–557.

**Bush, V. and J.P. Devlin** (1991) Spectra of dangling OH bonds in amorphous ice: Assignment to 2-and 3-coordinated surface molecules. *Journal of Chemical Physics*, **94**: 4091–9402.

**Chalmers, J.L.** (1952) Electric charges from ice friction. *Journal of Atmospheric and Terrestrial Physics* **2**: 337–339.

**Colbeck, S.C.** (1992) A review of processes that control snow friction. USA Cold Regions Research and Engineering Laboratory, Monograph 92–2.

**Colbeck, S.C.** (1994) Electrical charging of skis gliding on snow. *Medicine and Science in Sports and Exercise,* **27**(1): 136–141.

**del Pennino, U., A. Loria, S. Mantovani and E. Mazzega** (1974) Polarization phenomena induced by cracks in Ih ice crystals. *Nuovo Cimento,* **24**(1): 108–120.

**Elbaum, M., S.G. Lipson and J.G. Dash** (1993) Optical study of surface melting on ice. *Journal of Crystal Growth,* **129**: 491–505.

**Evans, D.B.C., J.F. Nye and K. Cheeseman** (1976) The kinetic friction on ice. *Proceedings, Royal Society*, *Series A,* **347**: 493–512.

**Evtushenko, A.A., V.F. Petrenko and I.A. Ryzhkin** (1984) Electric polarization of ice in nonuniform elastic strains. *Physica Status Solidi (a),* **86**: K31–K34.

**Evtushenko, A.A. and V.F. Petrenko** (1991) Investigations of the pseudopiezoelectric effect and the stress-potential constants of charge carriers in ice. *Soviet Physics–Solid State*, **33**(5): 850–855.

**Evtushenko, A.A., N. Maeno, V.F. Petrenko and I.A. Ryzhkin** (1987) Pseudopiezoelectric effect in ice. *Journal de Physique C1,* **48**(3): 109–113.

**Fifolt, D.A**. (1990) Preliminary investigation into the electrical properties of cracks in ice. In *Abstracts for Combined Meeting of the Advisory Panels of the ONR-Arctic Ice Ocean Dynamics and Mechanics Program at Dartmouth College and the University of Colorado and of the Ice Research Laboratory, June 19–20, Hanover New Hampshire.*

**Fifolt, D.A.** (1991) Study of electromagnetic emission from cracks in ice. MS Thesis, Thayer School of Engineering, Dartmouth College, Hanover, New Hampshire.

**Fifolt, D.A., Petrenko, V.F. and E.M. Schulson** (1992) Electrical signals from cracks in ice. In *Physics and Chemistry of Ice* (N. Maeno and T. Hondoh, Eds.). Sapporo: Hokkaido University Press, p. 470–475.

**Fifolt, D.A., V.F. Petrenko and E.M. Schulson** (1993) A preliminary study of electro-magnetic emissions from cracks in ice. *Philosophical Magazine B,* **673**: 289–99.

**Fletcher, N.H.** (1962) Surface structure of water and ice. *Philosophical Magazine,* **7**: 255.

**Fletcher, N.H.** (1963) Surface structure of water and ice—A reply and correction. *Philosophical Magazine,* **8**: 1425.

**Fletcher, N.H.** (1968) Surface structure of water and ice II. A revised model. *Philosophical Magazine* **18**: 1287.

**Fletcher, N.H.** (1970) *The Chemical Physics of Ice*. Cambridge: Cambridge University Press.

**Furukawa, Y., M. Yamamoto and T. Kuroda** (1987) Ellipsometric study of the transition layer on the surface of an ice crystal. *Journal of Crystal Growth,* **82:** 665–677.

**Glen, J.W.** (1974) The physics of ice. USA Cold Regions Research and Engineering Laboratory, Cold Regions Science and Engineering Monograph II-C2a.

**Glen, J.W.** (1975) Mechanics of ice. USA Cold Regions Research and Engineering Laboratory, Cold Regions Science and Engineering Monograph II-C2b.

**Gluschenkov, O.V. and V.F. Petrenko** (1993) Remote sensing of damage in ice using electromagnetic emission from cracks: theoretical background and preliminary experimental results. In *Ice Mechanics* (J. Dempsey et al., Ed.). New York: American Society of Mechanical Engineers, p. 97–111.

**Golecki, I. and C. Jaccard** (1978) Intrinsic surface disorder in ice near the melting point. *Journal of Physics C: Solid State Physics,* **11:** 4229–4237.

**Hellan, K**. (1984) *Introduction to Fracture Mechanics.* New York: McGraw-Hill Book Company.

**Higashi, A.** (1969) Mechanical properties of ice single crystals. In *Physics of Ice* (N. Riel et al., Ed.). New York: Plenum Press, p. 197–212.

**Hobbs, P.V**. (1974) *Ice Physics.* Oxford, England: Clarendon Press.

**Itagaki, K**. (1970) X-ray topographic study of vibrating dislocations in ice under an AC electric field. *Advances in X-ray Analysis,* **13**: 526–538.

**Itagaki, K**. (1978) Dielectric properties of dislocation-free ice. *Journal of Glaciology*, **21**(85): 207–217.

**Itagaki, K**. (1982) Charged dislocations in ice. II. Contribution to dielectric relaxation. USA Cold Regions Research and Engineering Laboratory, CRREL Report 82-7.

**Itagaki, K**. (1983) Possibility of anomalous relaxation due to the charged dislocation process. *Journal of Physical Chemistry,* **87**: 4261–4264.

**Jaccard, C.** (1964) Thermodynamics of irreversible processes applied to ice. *Physik der Kondensierten Materie*, **3**: 99–118.

**Joncich, D.M., J. Holder and A.V. Granato** (1978) Direct determination of an upper limit for the electrical charge on dislocations in ice. *Journal of Glaciology*, **20**(84): 543–546.

**Jones, D.E., F.E. Kennedy and E.M. Schulson** (1991) The kinetic friction of saline ice against itself at low sliding velocities. *Annals of Glaciology,* **15**: 242–246.

**Kachurin, L.G., N.O. Grigorov, Y.N. Kuzin, V.F. Psalomshchikov and I.A. Stepanyuk** (1979) Electromagnetic radiation from snow and ice, generated in dynamic processes. *Doklady Akademii Nauk SSSR, Geophysics,* **248** (3): 19–21.

**Kachurin, L.G., V.Y. Andrusenko, V.B. Loginov, V.F. Psalomshchikov, K.K. Ovanes'yan, and A.A. Khar'kov** (1988) Generation of electromagnetic fields by fracture of the ice cover of marine areas. *Izvestya, Atmospheric and Oceanic Physics,* **24**(10): 815–817.

**Kachurin, L.G., V.F. Psalomshchikov and I.A. Stepanyuk** (1984) Nonthermal radiation emission by deformed ice cover on water. *Issledovaniye Zemli iz Kosmosa*, no. 3, p. 60–65.

**Latham, J.** (1963) Electrification produced by asymmetric rubbing of ice on ice. *British Journal of Applied Physics,* **14**: 488–490.

**Latham, J. and B.J. Mason** (1961) Generation of electric charge associated with formation of soft hail in thunderstorms. *Proceedings, Royal Society A*, **260**: 537–549.

**MacDonald, J.R.** (1953) Theory of ac space-charge polarization effects in photoconductors, semiconductors, and electrolytes. *Physical Review*, **92** (1): 4–17.

**Mae, S. and A. Higashi** (1973) Effects of plastic deformation on the dielectric properties of ice. *Crystal Lattice Defects*, **4**: 295–308.

**Maeno, N.** (1973) Measurements of surface and volume conductivity of single ice crystals. *Physics and Chemistry of Ice* (E. Whalley, S. Jones and L.W. Gold, Ed.). Ottawa: Royal Society of Canada, pp. 140–143.

**Maeno, N.** (1981) *The Science of Ice*. Hokkaido University Press (in Japanese).

**Mizuno, Y. and N. Hanafuza** (1987) Studies of surface properties of ice using nuclear magnetic resonance. *Journal de Physique C1,* **48:** C1-511–C1-517.

**Noll, G.** (1978) The influence of the rate of deformation on the electrical properties of ice monocrystals. *Journal of Glaciology,* **21**(85) : 277–289.

**Nye, J.F.** (1985) *Physical Properties of Crystals*. Oxford, England: Clarendon Press.

**Ocampo, J. and J. Klinger** (1983) Modification of the surface structure of ice during aging. *Journal of Physical Chemistry,* **87**: 4167–4170.

**Osip'yan, Y.A., V.F. Petrenko, A.V. Zaretskii and R.W. Whitworth** (1986) Properties of II-VI semiconductors associated with moving dislocations. *Advances in Physics,* **35**(2): 115–188.

**Petrenko, V.F.** (1992) Applications of electrical signals from cracks to ice micromechanics. In *Proceedings of the IAHR Ice Symposium 1992, Banff, Alberta*. International Association for Hydraulic Research, vol. 2, p. 140–154.

**Petrenko, V.F.** (1993a) On the nature of electrical polarization of materials caused by cracks. Application to ice electromagnetic emission. *Philosophical Magazine B*, **67**(3): 301–315.

**Petrenko, V.F.** (1993b) Electrical properties of ice. USA Cold Regions Research and Engineering Laboratory, Special Report 93–20.

**Petrenko, V.F.** (1993c) Structure of ice. USA Cold Regions Research and Engineering Laboratory, Special Report 93-25.

**Petrenko, V.F.** (1993d) Laboratory and field study of electromagnetic emission from cracks in ice. Proposal submitted to National Science Foundation.

**Petrenko, V.F.** (1994a) The effect of static electric fields on ice friction. *Journal of Applied Physics* **76**(2): 1–4.

**Petrenko, V.F.** (1994b) The surface of ice. USA Cold Regions Research and Engineering Laboratory, Special Report 94-22.

**Petrenko, V.F. and S.C. Colbeck** (1995) Generation of electric field in ice and snow friction. *Journal of Applied Physics*, **77**(9): 4518–4521.

**Petrenko, V.F. and O.V. Gluschenkov** (1995) Measurements of crack velocity and electromagnetic emission from cracks in sea ice. In *Ice Mechanics, Proceedings of Joint Applied Mechanics and Materials Summer Conference AMD-MD'95, 28–30 June, Los Angeles* (J.M. Dempsey and Y.D.S. Rajapaksey, Ed.). New York: ASME, p. 201–210.

**Petrenko, V.F. and E.M. Schulson** (1992) The effect of static electric fields on protonic conductivity of ice single crystal. *Philosophical Magazine B*, **66:** 341–353.

**Petrenko, V.F. and E.M. Schulson** (1993) Action of electric fields on plastic deformation of pure and doped ice single crystals. *Philosophical Magazine*, **67**(1): 173–185.

**Petrenko, V.F. and I.A. Ryzhkin** (1984a) Dielectric properties of ice in the presence of space charge. *Physica Status Solidi* (b), **121**: 421–427.

**Petrenko, V.F. and I.A. Ryzhkin** (1984b) Theory of anelastic relaxation of ice. *Soviet Physics-Solid State,* **26**(9): 2681–2688.

**Petrenko, V.F. and I.A. Ryzhkin** (1986a) Anelastic relaxation and viscous deceleration of dislocation in ice. In *Abstracts of Vth International Conference on Properties and Structure of Dislocations in Semiconductors*, Moscow (Zvenigorod).

**Petrenko, V.F. and I.A. Ryzhkin** (1986b) The interac-

tion between dislocations and current carriers in ice. In *Abstracts of V<sup>th</sup> International Conference on Properties and Structure of Dislocations in Semiconductors*, Moscow (Zvenigorod).

**Petrenko, V.F. and N. Maeno** (1987) Ice field transistor. *Journal de Physique C1,* **48**: 115–119.

**Petrenko, V.F. and R.W. Whitworth** (1983) Electrical currents associated with dislocation motion in ice. *Journal of Physical Chemistry,* **87**: 4022–4024.

**Reynolds, S.E., M. Brook and M.F. Gourley** (1957) Thunderstorm charge separation. *Journal of Meteorology,* **14**: 426–436.

**Rossman, F.** (1950) Polare Kristallform und Electrische Erregung des Eises. *Experientia*, **6:** 182–184.

**Sato, A. and G. Wakahama** (1992) Measurement of the velocity of cracks propagation in ice. In *Physics and Chemistry of Ice* (N. Maeno and T. Kondoh, Ed.). Sapporo: Hokkaido University Press, p. 476–480.

**Takahashi, T.** (1966) Thermoelectric effect in ice. *Journal of Atmospheric Science,* **23:** 74–77.

**Takahashi, T.** (1969a) Electric potential of rubbed ice surface. *Journal of Atmospheric Science,* **26:** 1259–1265.

**Takahashi, T.** (1969b) Electrical charge generation by breaking of frost under a temperature gradient. *Journal of Meteorological Society of Japan,* **47**(1): 23–28.

**Takahashi, T.** (1983) Electric charge separation during ice deformation and fracture under a temperature gradient. *Journal of Physical Chemistry,* **87**: 4122–4124.

**Thiel, D.V**. (1992) Electromagnetic emission (EME) from ice crack formation: preliminary observations. *Cold Regions Science and Technology,* **21**: 49–60.

**Weyl, W.A.** (1951) Surface structure of water and some of its physical and chemical manifestations. *Journal of Colloid Science,* **6**: 389–405.

**Whalley, E. and D.D. Klug** (1984) Disorder-induced piezoelectric and piezo-optic effects. I. The theory of the piezoelectric properties and its application to ice. *Journal of Chemical Physics,* **81**(12): 6119–6123.

**Whitworth, R.W.** (1975) Charged dislocations in ionic crystals. *Advances in Physics,* **24** (2): 203–304.

**Workman, E.J. and S.E. Reynolds** (1949) Electrical activity as related to thunderstorm electricity. *Bulletin of the American Meteorology Society,* **30**: 142–144.

**Workman, E. and S.E. Reynolds** (1950) Electrical phenomena occurring during the freezing of dilute aqueous solutions and their possible relationship to thunderstorm electricity. *Physical Review,* **78**: 254–259.

**Yoshida, Z.** (1944) The mechanism of charge generation in friction and destruction of ice and in thunderclouds. *Low Temperature Science*, **A1**: 149–187.

**Zaretskii, A.V.** (1991) Experimental determination of the $H_3O^+$ ion's mobility in ice from 160 to 240K. In *Summaries of International Symposium on the Physics and Chemistry of Ice, September 1–6.* Sapporo, Japan, p. 204.


## SELECTED BIBLIOGRAPHY

**Bernal, J.D. and R.H. Fowler** (1933) A theory of water and ionic solutions with particular reference to hydrogen and hydroxyl ions. *Journal of Chemical Physics*, **1**: 515–458.

**Berri, B.L.** (1986) Electromagnetic processes in water crystallization and ice failure. In *Problems of Engineering Glaciology.* Nauka: Novosibirsk (USSR), p. 24–32.

**Berri, B.L. and V.A. Gribov** (1982) Radio irradiation of glaciers and snow avalanches. *Materiali Glatsiologicheskih Issledovanii*, **44**: 150–156.

**Bogorodskii, V.V., A.V. Gusev, V.A. Nikitin and M.B. Yartsev** (1990) On electromagnetic emission during dynamic processes in ice. *Doklady Akademii Nauk SSSR*, **314**(6): 1357–1360.

**Fifolt, D.A., V.F. Petrenko and E.M. Schulson** (1991) Electrical signals from cracks in ice. In *Summaries of International Symposium on the Physics and Chemistry of Ice, 1–6 September Sapporo, Japan*, p. 205–206.

**Itagaki, K.** (1979) Charged dislocations in ice. I. Existence and charge density measurements by X-ray topography. USA Cold Regions Research and Engineering Laboratory, CRREL Report 79-25.

**Pauling, L.** (1935) The structure and entropy of ice and of other crystals with some randomness of atomic arrangement. *Journal of American Chemical Society*, **57**: 2680–2684.

**Petrenko, V.F.** (1992a) Electromagnetic emission from cracks in polycrystalline ice. *Abstracts of AGU Spring Meeting, Montreal, May 12–16, 1992, supplement to EOS*, p. 308–309.

**Petrenko, V.F.** (1992b) On the nature of electrical signals from cracks in ice. In *Physics and Chemistry of Ice* (N. Maeno and T. Hondoh, Ed.). Sapporo: Hokkaido University Press, p. 175.

**Petrenko, V.F. and R.W. Whitworth** (1994) Structure of ordinary ice I$_h$. Part II: Defects in ice. Volume 1: Point defects. USA Cold Regions Research and Engineering Laboratory, Special Report 94-4.

# REPORT DOCUMENTATION PAGE

Public reporting burden for this collection of information is estimated to average 1 hour per response, including the time for reviewing instructions, searching existing data sources, gathering and maintaining the data needed, and completing and reviewing the collection of information. Send comments regarding this burden estimate or any other aspect of this collection of information, including suggestion for reducing this burden, to Washington Headquarters Services, Directorate for Information Operations and Reports, 1215 Jefferson Davis Highway, Suite 1204, Arlington, VA 22202-4302, and to the Office of Management and Budget, Paperwork Reduction Project (0704-0188), Washington, DC 20503.

| 1. AGENCY USE ONLY (Leave blank) | 2. REPORT DATE <br> February 1996 | 3. REPORT TYPE AND DATES COVERED |
|---|---|---|

**4. TITLE AND SUBTITLE**

Electromechanical Phenomena in Ice

**5. FUNDING NUMBERS**

DAAL-03-91-G-0164

**6. AUTHORS**

Victor F. Petrenko

**7. PERFORMING ORGANIZATION NAME(S) AND ADDRESS(ES)**

U.S. Army Cold Regions Research
and Engineering Laboratory
Hanover, New Hampshire 03755

Thayer School of Engineering
Dartmouth College
Hanover, New Hampshire 03755

**8. PERFORMING ORGANIZATION REPORT NUMBER**

Special Report 96-2

**9. SPONSORING/MONITORING AGENCY NAME(S) AND ADDRESS(ES)**

U.S. Army Research Office
Research Triangle Park, North Carolina

**10. SPONSORING/MONITORING AGENCY REPORT NUMBER**

**11. SUPPLEMENTARY NOTES**

For conversion of SI units to non-SI units of measurement consult *Standard Practice for Use of the International System of Units (SI)*, ASTM Standard E380-93, published by the American Society for Testing and Materials, 1916 Race St., Philadelphia, Pa. 19103.

**12a. DISTRIBUTION/AVAILABILITY STATEMENT**

Approved for public release; distribution is unlimited.

Available from NTIS, Springfield, Virginia 22161.

**12b. DISTRIBUTION CODE**

**13. ABSTRACT** (*Maximum 200 words*)

This report examines the electromechanical effects in ice. This group of physical phenomena, which was found and studied relatively recently, broadens basic knowledge of ice and may have some practical applications. The electromechanical phenomena in this report are separated into three groups: 1) Effects in which electromagnetic fields are generated by means of mechanical actions such as elastic stress, plastic strain, fracture or friction; 2) Effects in which an application of electric fields modifies such mechanical properties of ice as its plasticity, elasticity and friction; 3) Effects in which plastic strain changes electrical conductivity or dielectric permittivity of ice. Experimental results and theoretical models are discussed and some possible practical applications suggested.

**14. SUBJECT TERMS**

| | |
|---|---|
| Cracks in ice | Ice mechanics |
| Electrical properties | Ice physics |
| Ice defects | |

**15. NUMBER OF PAGES**
36

**16. PRICE CODE**

| 17. SECURITY CLASSIFICATION OF REPORT <br> UNCLASSIFIED | 18. SECURITY CLASSIFICATION OF THIS PAGE <br> UNCLASSIFIED | 19. SECURITY CLASSIFICATION OF ABSTRACT <br> UNCLASSIFIED | 20. LIMITATION OF ABSTRACT <br> UL |
|---|---|---|---|